# Moisture sources and dynamics over southeastern Tibetan Plateau reflected in dual water vapor isotopes

Zhongyin Cai[1*], Rong Li[1], Cheng Wang[1], Qiukai Mao[1], Lide Tian[1]

[1]Institute of International Rivers and Eco-security, Yunnan Key Laboratory of International Rivers and Transboundary Eco-security, Ministry of Education Key Laboratory for Ecosecurity of Southwest China, Yunnan University, Kunming, China

*Corresponding author: Zhongyin Cai (czypil@gmail.com and z.cai@ynu.edu.cn)

**Abstract**

The southeastern Tibetan Plateau (SETP) has experienced a significant drying trend in recent decades, likely linked to changes in moisture sources. Water vapor isotopes are valuable tracers of the atmospheric water cycle, yet their interpretation is hindered by ambiguities in atmospheric controls.~~The Tibetan Plateau (TP) serves as a water tower for major rivers in Asia, and mountain valleys in southeastern TP are key channels for moisture entering the TP. Water resources on the TP are experiencing spatially opposite changes due to climate change, and understanding the sources and dynamics of atmospheric moisture is vital.~~ To investigate the role of ocean surface evaporation, continental air mass intrusion, and rain-vapor interaction, we present a three-year daily time series of near-surface ~~water~~ vapor~~ isotope compositions (~~$\delta^{18}O$ and *d*-excess~~)~~ from the ~~South-East TP~~SETP station. ~~We find~~Our analysis reveals that apparent negative correlations between *d*-excess and relative humidity over the Indian Ocean are ~~mainly~~

~~reflect~~primarily driven by ~~their similar seasonality~~similar seasonal patterns, which become ~~. When analyzed for different seasons, the correlation is~~ insignificant or ~~only explains a~~ marginal ~~fraction of variance~~when examined seasonally. ~~Therefore,~~This result underscores the need for caution ~~is required when~~in interpreting ~~the~~ *d*-excess as a conservative tracer of ocean surface evaporation. Instead, we identify local and upstream specific humidity ~~is~~ as the ~~main~~ primary ~~factor determining~~determinant of non-monsoon season *d*-excess variability, ~~due to~~influenced by the intrusion of cold and dry air from upper levels. During the summer monsoon season, both *d*-excess and $\delta^{18}O$ ~~mainly~~ reflect the effect of raindrop evaporation ~~on humidity~~ during transport, which decreases ~~, lower vapor~~ $\delta^{18}O$ but increases *d*-excess ~~values~~. These findings provide new insights into the ~~significance of using~~use of water isotopes to track moisture sources and dynamics over the SETP, ~~with~~ particularly under varying ~~seasonally~~ seasonal ~~alternating~~ circulation systems. Particularly, the findings for *d*-excess will ~~improve~~contribute to our ~~the~~ understanding of different moisture sources and ~~guide~~ provide a framework for ~~the~~ interpreting ~~ation of~~ *d*-excess ~~derived from other water bodies~~in various hydroclimatic applications, including ~~and~~ ice core studies.

## 1 Introduction

The Tibetan Plateau (TP) and its surrounding regions, ~~also termed~~known as the Third Pole and the Asian Water Tower, ~~form the highest and largest plateau on Earth that influences climatic and hydrological systems at regional to global scales, such as the formation of the Asian Summer Monsoon (Wu et al., 2022; Yao et al., 2022). In addition, the TP stores the largest amount of frozen water outside of polar regions and sustains~~plays a crucial role in supplying water ~~freshwater supplies of~~ to major ~~river systems in~~Asian rivers~~Asia~~, including the Mekong, Salween, Ganges, Yarlung Zangbo, among others, sustaining ecosystems and populations across the continent (Immerzeel et al., 2020; Yao et al., 2022). ~~However~~In recent decades, the water balance on the TP has ~~experienced~~ undergone significant

changes under the backdrop of global warming (Yao et al., 2022). Notably~~For instance~~, the southeastern TP (SETP) is experiencing a drying trend while wetting in the north~~ern TP~~ (Jiang et al., 2023; Zhang et al., 2023; Yao et al., 2022). Atmospheric water vapor is the primary input to the hydrological system, making it essential to understand its sources and dynamics to diagnose regional water imbalances. ~~Atmospheric water vapor is the input of the water storage system and understanding its sources and dynamics is vital for understanding the imbalance of TP's hydrological system.~~Using a Lagrangian vapor tracking method, Zhang et al. (2023) suggested that the drying trend is associated with meteorological droughts propagating from moisture source regions. However, their conclusions and methodology are subjects of ongoing debate (Zhang et al., 2025; Zhao et al., 2025). –

Water stable isotopes are natural tracers of the water cycle, offering valuable insights into moisture sources and dynamics (Bowen et al., 2019; Galewsky et al., 2016). ~~and~~ These isotopes have been intensively studied on the TP in precipitation, surface water, and ice cores (Yao et al., 2013; Thompson et al., 2024; Bershaw, 2018). However, the interpretation of these isotopic signals remains challenging due to complex fractionation processes and shifting circulation systems between summer monsoon and westerlies.

~~In general, precipitation isotope ratios ($\delta^{18}O$ and $\delta^{2}H$) over the southern TP have lower values during the summer monsoon season and higher values during the non-monsoon season under the influence of the westerlies (He et al., 2015; Tian et al., 2007; Guo et al., 2024; Yang et al., 2017).~~ Recent studies have confirmed that monsoon convection at upstream along moisture transport pathways, rather than local precipitation amount, ~~is the key process that~~ controls summer monsoon season precipitation $\delta^{18}O$ over southern TP (Cai et al., 2017; He et al., 2015). This is related to the "amount effect" (Dansgaard, 1964), ~~Different processes have been proposed to elucidate the relationship between precipitation $\delta^{18}O$ and convection where the amount effect (Dansgaard, 1964) is present (Bowen et al., 2019; Galewsky et al., 2016). A relatively classical interpretation is that~~where higher precipitation leads to lower $\delta^{18}O$ values due to ~~the~~ continuous rainout associated with stronger convection ~~could cause depleted~~

~~precipitation,~~ following the Rayleigh distillation (Cai and Tian, 2016; Scholl et al., 2009; Vuille et al., 2003). Additionally, ~~Another interpretation emphasized the role of rain-vapor interaction~~interactions between rain and water vapor play a significant role ~~that partial evaporation of raindrops formed at higher altitudes isotopically~~in ~~depletes~~ depleting the lower tropospheric ~~water~~ vapor ~~and then affects subsequent precipitation isotope compositions~~isotopes (Risi et al., 2008a; Kurita et al., 2011; Cai et al., 2018; Lee and Fung, 2008). While the regional amount effect prevails during the monsoon season, this relationship weakens or reverses in the non-monsoon season when it is dominated by westerlies. This variability suggests additional controls such as moisture source variability, kinetic fractionation, or shifts in atmospheric circulation patterns (Breitenbach et al., 2010; Cai and Tian, 2020; Guo et al., 2024; Yao et al., 2013).

Observations of vapor isotope ~~compositions~~ could help disentangle the different processes involved in the amount effect, ~~especially~~ particularly through examining the secondary parameter deuterium excess (*d*-excess). The *d*-excess, ~~is~~ defined ~~as $\delta^2H - 8\delta^{18}O$~~ by Dansgaard (1964) as $\delta^2H - 8\delta^{18}O$, ~~and mainly~~primarily reflects the effects of kinetic fractionation. ~~The~~ During rainout process, ~~mostly involves~~ equilibrium fractionation is the dominant mechanism, whereas ~~while~~ raindrop evaporation is associated with kinetic fractionation~~, and they can therefore have different *d*-excess signatures in water vapor~~. Further, limited precipitation during non-monsoon seasons makes it challenging to study a full seasonal cycle of the atmospheric water cycle, which can be compensated by continuous monitoring of vapor isotopes. While a few stations on the TP have monitored ~~I~~isotopic compositions in the vapor phase~~ have only been observed at a few stations on the TP and isotope ratios (δ values) have been the major focus of previous studies~~ (Tian et al., 2020; Dai et al., 2021; Chen et al., 2024; Yu et al., 2016; Yu et al., 2015), ~~less is known~~there is limited knowledge about vapor *d*-excess.

~~It is less certain regarding what caused higher isotope ratios during the non-monsoon season. Following the regional amount effect (Galewsky et al., 2016; Bowen et al., 2019), high $\delta^{18}O$ values could be explained by~~

~~weakened convection during the non-monsoon season. However, precipitation $\delta^{18}O$ is lower during late- to post-monsoon season in regions extending from the southeastern TP to the head of the Bay of Bengal (BOB), which is not consistent with the weakening of convection (Breitenbach et al., 2010; Cai and Tian, 2020). Shifts of moisture transport pathways between convection active and non-active regions have been invoked to explain this abnormal seasonal pattern (Cai and Tian, 2020; Lekshmy et al., 2022). On the other hand, higher precipitation $\delta^{18}O$ accompanied by higher *d*-excess during the non-monsoon season has been interpreted as more intense continental recycling or moisture from the Mediterranean delivered by the westerlies compared with moisture from the Indian Ocean during the summer monsoon (Tian et al., 2007; Yao et al., 2013; An et al., 2017; Breitenbach et al., 2010). In addition, understanding of the atmospheric water cycle for a full seasonal cycle is complicated by the lack of precipitation during the non-monsoon season which can be compensated by monitoring atmospheric water vapor isotopes as it is not limited by precipitation events.~~

Both theoretical predictions and observations over ocean surfaces ~~suggested~~ indicate that *d*-excess reflects ocean surface evaporation conditions~~,~~ such as sea surface temperature (SST) and relative humidity normalized to SST ($RH_{SST}$) (Merlivat and Jouzel, 1979; Bonne et al., 2019; Liu et al., 2014; Craig and Gordon, 1965). These relationships are frequently invoked in interpreting~~Interpretations of~~ *d*-excess over the TP ~~also frequently invoke these relationships with ocean evaporation conditions~~ (Zhao et al., 2012; Shao et al., 2021; Chen et al., 2024; Liu et al., 2024). ~~However, relationships with either $RH_{SST}$ or SST are much weaker than those observed over ocean surface.~~ For instance, Shao et al. (2021) showed significant correlations between an ice core *d*-excess record ~~derived~~ from the central TP and $RH_{SST}$ over the northern Bay of Bengal (BOB) and Arabian Sea (AS). However, the correlation coefficient ~~is~~ was only -0.44 ~~and the slope between *d*-excess and $RH_{SST}$ is as steep as~~with a steep slope of -0.99‰ $\%^{-1}$. This contrasts with oceanic regions where t~~T~~he slope ~~over oceanic regions generally~~typically ranges from -0.3‰ $\%^{-1}$ to -0.6‰ $\%^{-1}$ ~~based on in-situ observations~~ (Bonne et al., 2019; Liu et al., 2014; Benetti et al., 2014;

Uemura et al., 2008), suggesting additional complexities over terrestrial areas. Moreover, m~~M~~any studies have suggested that *d*-excess at terrestrial sites is not a conservative tracer of evaporation conditions ~~at~~ from ~~the~~ oceanic source regions (Fiorella et al., 2018; Aemisegger et al., 2014; Welp et al., 2012; Wei and Lee, 2019; Samuels‐Crow et al., 2014). ~~Besides temporal variations~~In addition, ice core *d*-excess values at high altitudes ~~are~~ are generally higher than ~~that~~ those observed in precipitation at lower altitudes on the TP (Shao et al., 2021; Tian et al., 2001; Zhao et al., 2012; Joswiak et al., 2013; Zhao et al., 2017; Thompson et al., 2000). The reason for this discrepancy remains unclear, ~~It is still unclear what caused the abnormally high *d*-excess in these high-altitude ice cores relative to precipitation and river isotope observations at lower altitudes~~highlighting the need for further research to understand the mechanism driving these differences.

Mountain valleys in the ~~southeastern TP~~SETP are ~~believed to be~~considered significant~~major~~ ~~moisture transport channels~~pathways for ~~delivering water vapor toward the TP~~transporting water vapor into the TP (Araguás-Araguás et al., 1998; Tian et al., 2007; Yao et al., 2013). ~~Therefore~~To investigate these processes, we initiated~~started~~ a water vapor sampling campaign at the South-East Tibetan Plateau Station for integrated observation and research of alpine environment (SETP station) in June 2015. We aim to study the moisture sources and dynamics and their ~~influence~~ influence on ~~water~~ vapor isotope compositions across different seasons. To achieve these goals, we explored the relationships between vapor isotopes and oceanic evaporation conditions, continental air mass intrusions, as well as rain-vapor interactions during different seasons. Finally, we discuss the implications of our findings for interpreting ice core records. ~~Following the previous study (Yao et al., 2013), we define June-September (JJAS) as the summer monsoon season. In contrast, we define November-April (Nov-Apr) as the non-monsoon season and May and October as the transition between the two seasons. We will show distinct seasonal moisture sources and dynamics between the two seasons as reflected in our vapor isotope observations and Lagrangian moisture source diagnostic. Our results suggest that the apparent correlation between SETP vapor *d*-excess and oceanic surface evaporation~~

~~conditions is mainly a result of their similar seasonality. Alternatively, we suggest the intrusion of dry and cold air by the westerlies from high altitudes contributes to high *d*-excess. In contrast, vapor $\delta^{18}O$ and *d*-excess confirm the significant role of rain-vapor interaction in the amount effect during the summer monsoon season.~~

## 2 Data and methods

### 2.1 Atmospheric water vapor sampling

~~Atmospheric water v~~Vapor samples were collected at the SETP station (29°46'N, 94°44'E, 3326 m above sea level, and Fig. S1) using a cryogenic trapping method ~~at the SETP station (29°46'N, 94°44'E, 3326 m above sea level, and Fig. S1)~~. The sampling system includes an air pump ~~pumping ambient air into the~~ , ~~cold trap,~~ a linked-ball-shaped glass cold trap, and an electric-powered system that creates and maintains a cold environment filled by 95% ethanol as cold as below -80 °C. Ambient air was pumped from an inlet ~~at approximately~~positioned about 8 m above ground level through a Teflon tube to a glass trap maintained ~~immersed in a cold environment with a~~at an operational temperature of~~at~~ -70 °C. The airflow rate was ~~adjusted~~ set to ~5 L/min, ~~to~~ allowing the collection of 10-20 ml of water samples ~~throughout~~ during each sampling session~~operation~~. Sampling durations were adjusted seasonally: ~~During summers, the duration of each sampling operation is~~ 24 hours in summer and extended to 48 hours in winter when necessary to ensure adequate sample volume. ~~During dry winters, however, we increased the sampling duration to 48 hours if a 24-hour sampling period cannot guarantee enough sample amount. The s~~Samples were collected at 20:00 Beijing Standard Time (12:00 UTC). The efficiency of ~~extracting water vapor from ambient air~~the trapping method was ~~tested~~ verified by connecting an additional cold trap to the ~~outlet of the initial cold trap~~system, which showed ~~and~~ no visible condensation ~~was noticed~~ in the additional cold trap (Yu et al., 2015). Further ~~comparison~~ validation was achieved through comparisons with~~against~~ direct measurements ~~of vapor isotope composition by the~~using a Picarro L2130-i Cavity Ring Down Spectroscopy (CRDS) at Lhasa, southern TP, ~~also~~

~~confirmed~~confirming the reliability of this method ~~in~~ for ~~sampling~~ atmospheric water vapor samplingover the TP (Tian et al., 2020).

The sampling campaign ~~was started on~~ran from 25 June 2015 ~~and ended on~~to 14 June 2018~~. In total~~, yielding a total of 742 samples~~ were collected.~~. These~~and all the collected~~ samples were ~~kept~~ stored frozen until ~~transportation to the laboratory for measurements~~analysis. Samples collected before 28 June 2016 were measured at the Key Laboratory of Tibetan Plateau Earth System, Environment and Resources, Institute of Tibetan Plateau Research, Chinese Academy of Sciences by a Picarro L2130-i analyzer. Samples collected after 28 June 2016 were measured at the Institute of International River and Eco-security, Yunnan University by a Picarro L2140-i analyzer. The isotopic values ~~are~~were calibrated using three standard waters, with detailed calibration procedures described by Liu et al. (2024). ~~and~~ The measurements are expressed relative to Vienna Standard Mean Ocean Water 2 (VSMOW2)~~. The precisions of measurements at both laboratories are~~, with precisions of 0.1‰ for $\delta^{18}O$, 0.4‰ for $\delta^{2}H$, and 1.2‰ for *d*-excess.

## 2.2 Meteorological data

Daily local meteorological data ~~before~~ prior to 2018, including precipitation amount, air temperature, air pressure, and relative humidity~~,~~ at the SETP station, were ~~provided by the station at~~obtained from the National Tibetan Plateau~~-~~/Third Pole Environment Data Center (Luo, 2018). Specific humidity (*q*) at the SETP station ~~is~~ was calculated ~~from~~ using air temperature, air pressure, and relative humidity ~~at the station~~data following established equations outlined in (Huang, 2018). Consistent with Yao et al. (2013), we defined June-September (JJAS) as the summer monsoon season. In contrast, November-April (Nov-Apr) was designated as the non-monsoon season, with May and October considered transition periods between the two seasons.

~~To facilitate analyses on larger spatial scales, w~~We further obtained meteorological variables ~~( such as including~~ 2-meter air temperature, 2-meter dew point temperature, ~~and~~ SST, ~~etc.)~~and others at 0.25°×0.25° and hourly

resolution from the European Centre for Medium-Range Weather Forecasts fifth generation reanalysis (ERA5) (Hersbach et al., 2019). $RH_{SST}$ is estimated ~~from~~ using ERA5 ~~2-meter meteorological data and SST~~data ~~using:~~ $RH_{SST} = e_{air}/e_{sat}$, where $e_{air}$ is vapor pressure of air and $e_{sat}$ is saturation vapor pressure with respect to SST. Additionally, ~~We further obtained~~ precipitation data at 0.1°×0.1° and half-hourly resolution were obtained from the Integrated Multi-satellitE Retrievals for GPM (V07) dataset (Huffman et al., 2023). ~~In addition~~Moreover, meteorological data at 1°×1° and 3-hourly resolution from the Global Data Assimilation System (GDAS) ~~are~~ were used to calculate ~~air mass~~backward trajectories (see ~~s~~Section 2.4 for details).

Statistical analyses primarily involved linear correlations and regressions, with the coefficient of determination ($R^2$) used to quantify the variance explained by each variable. In addition, we also used composite analysis to reveal relationships between variables. For example, to identify general patterns in backward trajectories associated with *d*-excess exceeding 30‰, all the days with such high *d*-excess were compiled into a collection. A composite map of trajectories from this collection was then constructed to reveal typical pathways under these conditions.

### 2.3 Theoretical framework for the understanding of isotope compositions and humidity

Besides complex atmospheric circulation models, the evolution of vapor isotope compositions during different moistening and dehydration processes can be ~~understood~~ predicted ~~by~~ through a compilation of atmospheric processes~~,~~ such as condensation, mixing, and raindrop evaporation~~, that lead to different pathways of isotopic evolution along atmospheric humidity~~ (Noone, 2012; Worden et al., 2007; Galewsky et al., 2016). These process shape distinct pathways of isotopic evolution in relation to atmospheric humidity.

The Rayleigh distillation model describes ~~T~~the progressive condensation of water vapor ~~and removal as rain droplets or ice is best described by the canonical Rayleigh distillation model~~ (Dansgaard, 1964). ~~In the Rayleigh distillation framework, condensate is removed from the air mass as soon as it forms, and t~~The isotope ~~ratio~~ composition of remaining vapor, denoted as $\delta$, ~~is described~~can be expressed as $\delta = (1 + \delta_0)(q/q_0)^{\alpha-1} - 1$,

where~~–~~ $q$ is the specific humidity, and $\alpha$ is the fractionation factor. A subscript of 0 refers to the initial condition of the air mass. ~~The falling r~~Raindrop evaporation introduces further complexity.~~may partially evaporate or exchange isotopes with ambient vapor.~~ As raindrops ~~are formed~~form at higher altitudes where ~~water~~ vapor is depleted in heavy isotopes, ~~the~~ their partial evaporation~~ of raindrops would preferentially deplete its~~affects the surrounding~~ water~~ vapor, leading to isotope values lower than those predicted by Rayleigh models~~ but increase the atmospheric humidity, which leads to values lower than that predicted by the Rayleigh distillation~~ (Risi et al., 2008a; Worden et al., 2007). The~~ evolution of along with under partial evaporation of raindrops can be described in~~is effect gives rise to~~ a~~ "super-Rayleigh" ~~trajectory~~ trajectories, characterized by an inflated~~ting~~ ~~the~~ effective fractionation factor ($\alpha_e$), defined as $\alpha_e = (1 + \phi)\alpha$, where $\phi$ quantifies ~~the degree to which deviates~~deviations from equilibrium. ~~We note that~~Notably, Worden et al. (2007) and Noone (2012) have given different equations ~~to quantify the deviations of from under different degrees of raindrop evaporation~~for such deviations, and ~~the same deviation of from requires very different degrees of raindrop evaporation. In this study, we follow~~this study aligns with the formulations by Noone (2012).

~~Finally, the~~Air mass mixing also influence~~ of air mass mixing on~~s humidity and isotopic compositions ~~can be modeled~~ through ~~the~~ mass balance ~~perspective~~principles. When ~~considering mixing~~ a dry air mass mixes with a moist ~~air mass~~one, ~~for instance,~~ the specific humidity of the mixed air~~ mass~~ can be described as $q = f_{dry}q_{dry} + f_{moist}q_{moist}$, where $f$ ~~is~~ represents the fraction of each air mass, with $f_{dry} + f_{moist} = 1$~~the subscript denoting different air masses and~~. Isotopic compositions ~~of the mixed air mass can be~~are similarly derived ~~similarly~~ by solving ~~the~~ mass balance equations for the light and heavy isotopes, ~~respectively. The outcome of the mixing process leads to~~resulting in a hyperbolic relationship between $\delta$ and $q$. In other words, $\delta \times q$ and $q$ should have a linear relationship in the mixing process (Fiorella et al., 2018). ~~In a framework of the Keeling plots (Keeling, 1958), the~~ The intercept of the regression between $\delta$ and $1/q$ or the slope between $\delta \times q$ and $q$ ~~gives~~ provides an

~~estimation~~ estimate of the moist end member's isotope composition~~.~~ (Keeling, 1958)~~of the moist end member~~.

Assuming a surface temperature of 25 °C and relative humidity of 85%, ~~following~~ we utilize the evaporation model by Craig and Gordon (1965) ~~we can derive that~~to determine the isotopic composition of ocean evaporation. This results in $\delta^{18}O$ ~~of ocean surface evaporation is~~= -11.5‰, $\delta^{2}H$ = -81.4‰, and *d*-excess = 10.6‰. ~~We use this isotopic signature of evaporated water vapor~~These values serve as ~~a~~ the wet end member ~~to model the~~for modeling moistening process through~~by~~ mixing with ocean ~~surface~~ evaporation. For the dry end member, we consider a dehydrated air mass ~~A hypothetical dry end member~~ from the Rayleigh curve at $q$ = 0.5 g/kg, $\delta^{18}O$ = -60.3‰, and $\delta^{2}H$ = -418.0‰ ~~is chosen to represent the dehydrated dry air~~(Fig. S2). The dehydration process ~~by~~ via condensation ~~is modeled~~is initiated at ~~by choosing a starting point at the mixing line with~~ a relative humidity of 80% on the mixing line. Similarly, ~~the~~ "super-Rayleigh" distillation ~~with~~ involving partial rain evaporation ~~is started from~~also begins from ~~the same~~this starting point. We explore two ~~For the cases of~~ "super-Rayleigh"~~, we simulated the isotopic evolution under two~~ scenarios: ~~(~~Rain_evap_A assumes 2% rain evaporation, while ~~and~~ Rain_evap_B~~).~~ assumes 5%, based on ~~Following the~~ equations from~~in~~ Noone (2012)~~, Rain_evap_A represents that 2% of rain is evaporated and Rain_evap_B represents an evaporated fraction of 5%~~. Additionally, we consider the influence of ~~Mixing with~~ evapotranspiration over south Asia and the TP ~~is another way that could modify the~~on atmospheric humidity and vapor isotope compositions over ~~southeastern~~ SETP. ~~Accurate q~~Quantify~~ication~~ng ~~of the~~ isotopic compositions of land surface evapotranspiration is challenging. Given ~~that~~ ~~the~~ precipitation $\delta^{18}O$ over south Asia ~~is~~ generally ~~between~~ ranges from -1.0‰ ~~and~~ to -5.0‰ (Bowen and Wilkinson, 2002; Terzer-Wassmuth et al., 2021) and transpiration ~~may account~~ constitutes two-thirds or more of evapotranspiration ~~or more~~ (Cao et al., 2022; Han et al., 2022; Good et al., 2015), we assume ~~the~~ a $\delta^{18}O$ value of -5.0‰ as an upper bound for land surface evapotranspiration ~~has a value of -5.0‰ as an upper bound~~. Similarly, we assume ~~that the~~a *d*-excess of 15.0‰ for this~~e~~ wet end member ~~of land surface evapotranspiration is 15.0‰~~.

## 2.4 ~~Air mass~~Backward trajectory and moisture source diagnostic

~~Air mass backward trajectories were calculated t~~To investigate ~~the~~ air mass transport and diagnose moisture sources and ~~transport~~ pathways toward SETP, we calculated backward trajectories using the Hybrid Single-Particle Lagrangian Integrated Trajectory model (HYSPLIT) (Stein et al., 2015). Trajectory calculations ~~is~~ were driven by ~~the~~ meteorological data ~~of~~ from the GDAS. ~~We released a~~Air parcels were released from 5 locations ~~(~~: the ~~studied~~ study site and points displaced 0.2° in each cardinal direction ~~) at~~. These releases occurred at 7 different vertical levels ~~at~~: 10, 50, 100, 200, 300, 400, and 500 m above ground level. For each day during the sampling campaign, trajectories were initiated every 3 hours to calculate 10-day backward trajectories ~~. In this setting,~~, resulting in 280 trajectories ~~were derived for each single~~per day. Geographical and meteorological variables, including location, pressure, temperature, specific humidity, rainfall amount, boundary layer height, and ~~the~~ terrain height along the trajectories, were stored at hourly intervals.

To quantify m~~M~~oisture contributions along ~~air mass~~ trajectories to ~~the humidity at~~ SETP's humidity, ~~is quantified using~~we applied the Lagrangian moisture source diagnostic method ~~of~~ developed by Sodemann et al. (2008). ~~The~~ This method ~~considers~~ uses mass balance principles along ~~the~~ trajectories. ~~and assigns~~interpreting increases in specific humidity (forward in time) as moisture uptake~~,~~ and decreases ~~in specific humidity~~ as moisture ~~lost~~ loss due to precipitation. ~~The method~~It also ~~proportionally considers~~accounts for the ~~decreased~~ reduced contribution of ~~early~~ earlier moisture uptake due to ~~the~~ precipitation en route. We ~~have~~ previously adapted this method to ~~quantify the~~identify moisture sources for ~~of~~ precipitation in sub-regions of South Asia and East Asia (Cai et al., 2018; Cai and Tian, 2020).

The diagnostic results ~~suggest~~ indicated that ~~the~~ approximately 5% of the moisture arriving at SETP remained unattributed ~~fraction of moisture arriving at SETP is ~5%, and therefore~~, confirming that 10-day trajectories are ~~capable of diagnosing most of the~~sufficient to diagnose most moisture sources. Unlike previous applications focused

on ~~Instead of focusing on quantifying~~identifying ~~the~~ evaporative moisture sources from the Earth's surface, ~~in this study, we focus on~~this study emphasizes the contribution of ~~the~~ air parcels ~~itself~~ themselves to ~~the humidity at SETP~~SETP's humidity. This variable is readily available from the diagnostic method, ~~and the~~where changes in~~of~~ air parcel contributions within the boundary layer between time steps ~~within the boundary layer is the~~represent moisture uptake from the ~~Earth~~ surface.

The moisture contribution ~~by~~ of an air parcel to SETP's humidity ~~at SETP gives~~ is a measure of the importance of upstream air ~~masses~~. We calculated weighted-mean values for key variables by using the moisture contribution of the air parcel along trajectories~~Using this variable~~ as the weight~~, mean upstream geographical and meteorological variables are hence calculated as weighted means~~. We also applied K-means clustering to group ~~cluster analysis on the~~ trajectories, helping to ~~visualize the~~identify major transport pathways ~~using the K-means clustering method~~. When calculating the mean trajectory for each cluster and meteorological variables along each mean trajectory, the moisture contribution ~~by~~ of the air parcel is also considered as the weight to calculate ~~weighted~~ weighted-means.

## 3 Results

### 3.1 General characteristics of vapor $\delta^{18}O$, *d*-excess, and local meteorological variables

In general, ~~water vapor~~ $\delta^{18}O$ values are at ~~a~~ lower levels during the summer monsoon season and ~~a~~ higher levels during the non-monsoon season (Fig. 1a). Mean~~–~~ ~~vapor~~ $\delta^{18}O$ values are -18.4‰ for the non-monsoon season, -23.3‰ for the summer monsoon season, -16.9‰ for May, and -22.8‰ for October. ~~During the onset of the summer monsoon, the vapor~~ $\delta^{18}O$ shows a dramatic decrease ~~to lower values~~at the onset of the summer monsoon. Conversely, from the end of the summer monsoon season to spring and early summer, ~~Without a sharp rebound to values before the summer monsoon, the~~ $\delta^{18}O$ ~~value~~ shows a gradual increase trend ~~from the end of the summer monsoon season toward the highest values during spring and early summer~~. Although the amount effect significantly influences this

region ~~is significantly influenced by the amount effect~~, the seasonal variation~~trend~~ of ~~vapor~~ $\delta^{18}O$ does not strictly ~~follow the seasonal variation of~~align with local precipitation patterns. For instance, while local precipitation ~~shows clear cessation~~ceases clearly after the summer monsoon (Fig. 1e), ~~while~~ $\delta^{18}O$ ~~does not rebound to the level before summer monsoon onset~~remains at relatively low levels. ~~These seasonal characteristics of vapor $\delta^{18}O$~~This behavior is consistent with precipitation $\delta^{18}O$ ~~observed~~ in ~~southeastern~~ SETP, northeast India, and Bangladesh (Yao et al., 2013; Cai and Tian, 2020; Yang et al., 2017).

In contrast to $\delta^{18}O$~~Overall~~, ~~water vapor~~ *d*-excess displays different seasonal dynamics. ~~also has lower~~The *d*-excess values ~~during~~ are lower during the summer monsoon season and higher ~~values~~ during ~~the~~ non-monsoon ~~season~~ periods (Fig. 1b). Mean ~~vapor~~ *d*-excess values are 18.3‰ for the non-monsoon season, 11.9‰ for the summer monsoon season, 13.7‰ for May, and 14.9‰ for October. However, the timing of ~~the~~ seasonal transitions ~~of~~ in ~~vapor~~ *d*-excess ~~is different~~differs from that of ~~vapor~~ $\delta^{18}O$. The highest ~~vapor~~ *d*-excess values generally occur during winter months when ~~the~~ air temperature and relative humidity (RH) are at their lowest levels (Fig. 1c and 1d). Furthermore, ~~and the~~ *d*-excess starts to decrease ~~from~~ in spring ~~which is,~~ earlier than the sharp drop ~~of~~ in ~~vapor~~ $\delta^{18}O$ ~~during~~ at the onset of the summer monsoon.

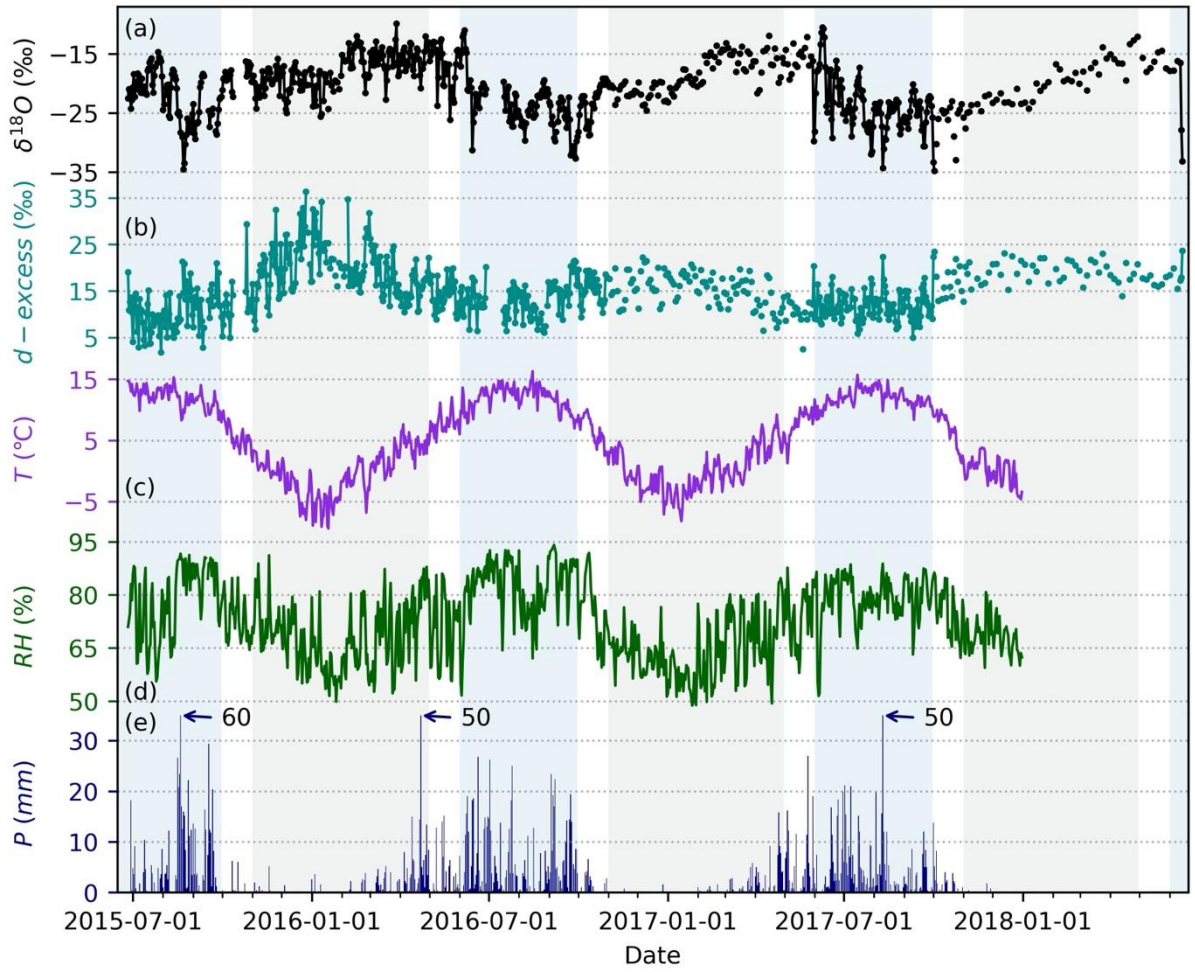


297

298 **Figure 1. ~~The general temporal variability~~Time series of observed ~~water~~ vapor δ$^{18}$O,~~isotope~~**

299 **~~compositions~~ *d*-excess, and daily local meteorological variables from 2015-2018: (a) δ$^{18}$O, (b) *d*-excess, (c) air**

300 **temperature, (d) relative humidity (RH), and (e) precipitation amount. ~~The l~~Light blue shading highlights**

301 **the summer monsoon season, ~~and the~~while light steel blue shading highlights the non-monsoon season.**

302 The linear relationship between paired δ$^{18}$O and δ$^{2}$H values, along with their ~~data points and~~ position~~their~~

303 ~~locations~~ relative to the global meteoric water line (GMWL, $\delta^2H = 8\delta^{18}O + 10$) (Craig, 1961), ~~generally~~ provides

304 additional insights into isotopic fractionation processes (Putman et al., 2019). The local ~~meteoric water~~vapor line

305 (~~LMWL~~LVL), estimated from all ~~vapor~~ δ$^{2}$H and δ$^{18}$O data points, is $\delta^2H = 7.96\delta^{18}O + 14.04$ ($R^2 = 0.98$). This

306 LVL ~~which~~ plots above but approximately parallel with the GMWL. This relatively higher intercept of ~~vapor LMWL~~

307 LVL reflects the continental location of the site and ~~further~~ additional kinetic fractionation after ocean ~~surface~~

evaporation. The $\delta^2H$-$\delta^{18}O$ relationship also varied seasonally. During the non-monsoon season, ~~T~~the ~~vapor LMWL~~ LVL ~~for non-monsoon season~~ is $\delta^2H = 7.58\delta^{18}O + 10.61$ ($R^2 = 0.96$), while during the ~~and for~~ summer monsoon season, it shifts to ~~is~~ $\delta^2H = 7.53\delta^{18}O + 0.91$ ($R^2 = 0.99$). Non-monsoon ~~season vapor isotope compositions mainly~~data primarily plot above both the GMWL and ~~even above~~ the overall ~~vapor LMWL~~LVL. Conversely, ~~While the majority~~ most ~~of~~ monsoon season isotope data ~~plot~~ fall below the overall ~~vapor~~ LV~~MW~~L, ~~those data points that have~~though the lowest ~~δ~~ δ-value~~s~~ ~~plot~~ points during this period are positioned above the overall ~~vapor LMWL~~ LVL, ~~indicating further~~suggesting additional kinetic fractionation such as rain evaporation (He et al., 2024). Vapor isotope ~~compositions~~ for May ~~are more similar to~~resemble those ~~during~~ of the non-monsoon season but ~~plot closer to~~align more closely with both the GMWL and ~~LMWL~~LVL, ~~while~~ whereas data for October ~~show a more~~exhibit ~~similar~~ behaviors similar to~~with~~ the monsoon season observations.

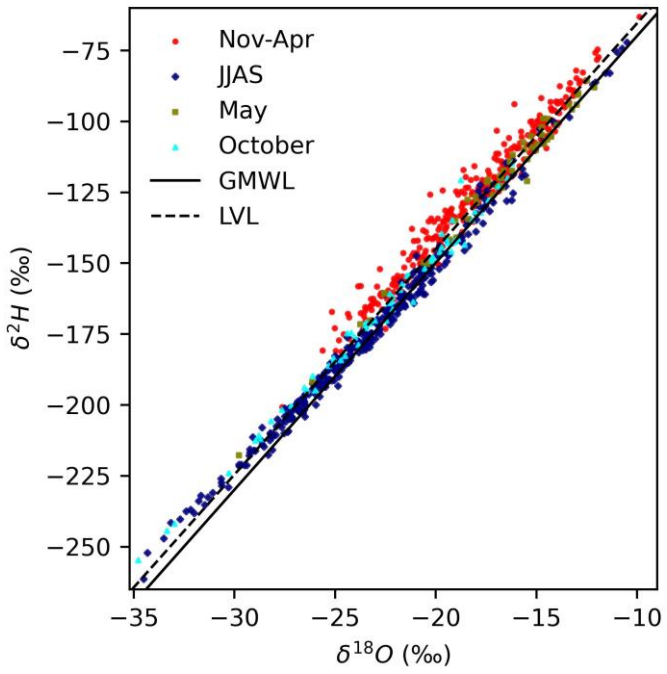

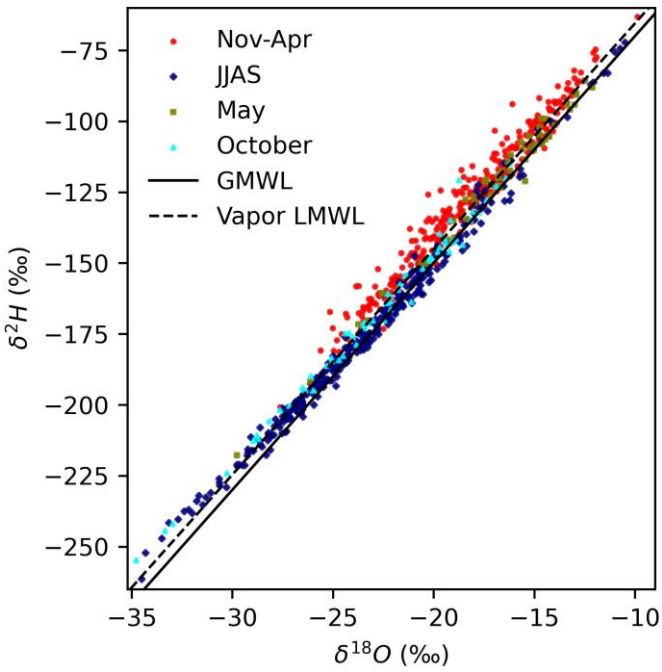


**Figure 2. Relationship between vapor δ²H and δ¹⁸O. The data is presented for different seasons: ~~Data during the~~ non-monsoon ~~season~~ (Nov-Apr) as red dots, ~~the~~ summer monsoon ~~season~~ (JJAS) as navy diamonds, May as olive squares, and October ~~are shown as red dots, navy diamonds, olive squares, and~~ cyan trangles~~, respectively~~. The solid line indicates the global meteoric water line (GMWL). The dashed line indicates the local ~~meteoric water~~vapor line (~~LMWL~~LVL) estimated from all ~~vapor~~ δ²H and δ¹⁸O data points.**

The relationships between ~~vapor~~ δ¹⁸O and specific humidity ($q$) further indicate distinct seasonal patterns in~~seasonally contrasting~~ moisture dynamics (Fig. 3a). ~~Note that only data before 2018 are shown as local meteorological data are unavailable in 2018. In addition, the sampling frequency during 2018 was reduced (Fig. 1) due to logistic issues. Therefore, when analyzing relationships between vapor isotope compositions (δ¹⁸O and *d*-excess) and meteorological variables (both locally and regionally) we only focused on data before 2018~~Due to unavilability of local meteorological data for 2018, our analyses focused on data collected before this year.. ~~For months d~~During the non-monsoon season, particularly in winter months, ~~the majority of~~most data points ~~fall~~ are positioned above the Rayleigh distillation line but below ~~the~~ a mixing line that ~~of~~ represents ~~an~~ an upper bound of hypothetical evapotranspiration over South Asia~~, especially for the winter months~~. This suggests a mix between a

dry end member and a moist end member. In contrast, ~~data for~~during the summer monsoon season, ~~months~~ data predominately fall below the Rayleigh ~~distillation~~ line, influenced ~~and are constrained~~ by "super-Rayleigh" ~~lines with different degrees of~~processes linked to rain evaporation.

Futher insights come from examing $\delta \times q$ ~~The relationships between~~ versus~~and~~ $q$ relationships, which highlight ~~further indicate~~ seasonal contrasts in moisture source signatures (Fig. S3). ~~Distribution of non-monsoon season and suggests the mixing between a dry end member that has almost totally dehydrated through condensation and a moist end member of surface evaporation or moisture that has been partially dehydrated through Rayleigh distillation (Fig. S3).~~ For the non-monsoon season, a~~A~~ simple estimation through the linear regression between $\delta \times q$ and $q$ suggests a $\delta^{18}$~~O of the~~ moist end member ~~for the non-monsoon season is~~with an $\delta^{18}$O of -13.9‰ ± 0.6‰. The amount weighted annual mean precipitation $\delta^{18}$O at ~~this~~ our site was about -14.5‰ (Yao et al., 2013). However, during the monsoon season, the overall estimation of $\delta^{18}$O for the moist end member through the linear regression between $\delta \times q$ and $q$ ~~for the summer monsoon season suggests $\delta^{18}$O of the moist end member is~~is significantly lower at -30.9‰ ± 1.8‰, pointing to ~~which is much lower than the estimation for the non-monsoon season. This exceptionally low value requires~~ an additional moisture source ~~of~~ from rain evaporation that is ~~much~~ more depleted in heavy isotopes ~~than surface evapotranspiration and is consistent with the distribution of $\delta^{18}$O-$q$ below the Rayleigh distillation line (Fig. 3a)~~. These results align with the distribution of $\delta^{18}$O-$q$ data below the Rayleigh line during the summer monsoon season (Fig. 3a), underscoring the influence of different moisture sources and processes across seasons.

The relationships between ~~vapor~~ $d$-excess and $q$ also ~~suggest~~ reflect seasonal contrasts in moisture dynamics (Fig. 3b). During non-monsoon season months, ~~vapor $d$-excess shows~~ a negative correlation is observed where lower ~~with $q$,~~ corresponds to~~and the highest~~ higher $d$-excess values (Figs. 1 and 3b). This relationship is particularly pronounced under dry and cold conditions ~~are generally associated with the driest and coldest air (Figs. 1 and 3b)~~.

In contrast, during the summer monsoon season, ~~However~~no clear relationship between~~,~~ ~~vapor~~ *d*-excess ~~does not show a clear relationship with~~and *q* is apparent, with *d*-excess~~and~~ ~~shows~~ showing ~~a substantial~~considerable variability ~~(~~of approximately 20‰~~ in range)~~ at any given *q* ~~during the summer monsoon season~~. These ~~relationships~~ findings suggest that ~~vapor~~ *d*-excess is less predictable ~~by~~ using *q* compared to~~than~~ $\delta^{18}O$, except ~~for~~ under low humidity levels.

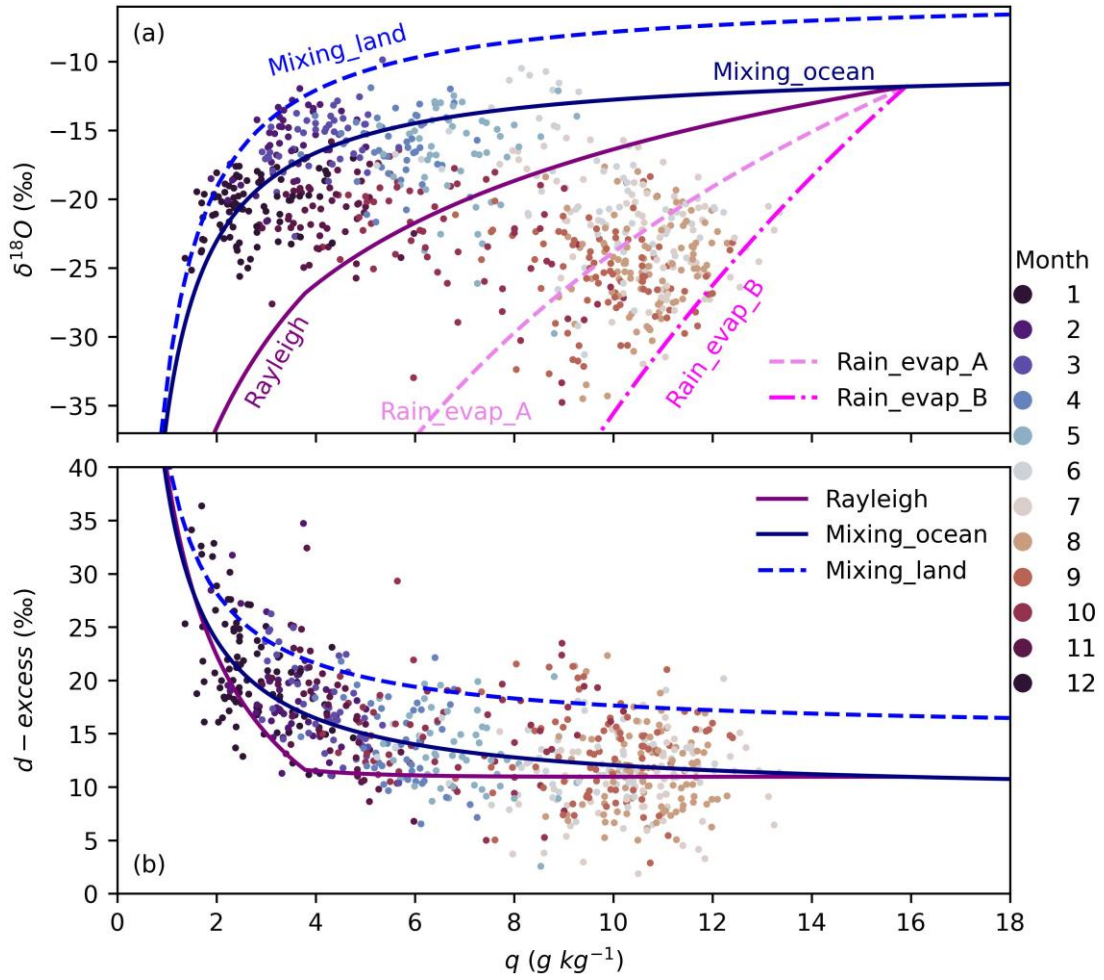


**Figure 3. Relationships between vapor isotopes ($\delta^{18}O$ and *d*-excess) and~~isotope compositions and~~ specific humidity (*q*) from 2015-2017. (a) scatter plot of $\delta^{18}O$ against ~~specific humidity (*q*)~~. (b) scatter plot of *d*-excess against *q*. Each data point is color-coded by month.~~The months for the data points are color-coded.~~ ~~The~~ ~~r~~Reference lines ~~are the same as~~correspond to those in Fig. S2~~,~~; ~~and~~ their interpretations ~~of these reference lines are referred to~~ is detailed in Fig. S2 and ~~s~~Section 2.3. Note that only data before 2018 are shown (see

text for details).

### 3.2 Seasonal variability in mMoisture sources and transport pathways for different seasons

To understand the drivers of behind the seasonal contrasting variations in moisture dynamics reflected in vapor isotope compositions, we first analyzed the moisture sources and transport pathways during different seasons (Fig. 4). Note again that weOur focus was on the contribution by of moisture from historical air masses (last 10 days) air mass to humidity at SETP instead of moisture uptake from the Earth surface.

During the non-monsoon season, moisture is mainly transported by via two pathways: branches with one originating from the west of SETP, carried by the westerlies (clusters Nov-Apr2 and Nov-Apr3), and the another from the south of SETP, such as the BOB (cluster Nov-Apr1). Quantitatively, the fraction of moisture from the south pathway and the sum of the two west branchescontributions frm these pathways are is comparable, with (52.4% from the southern pathway and vs. 47.7% from the western branches combined). Interestingly, We note that if moisture contributions by air parcels are not consideredwhen considering only trajectories without accounting for moisture contributions, trajectories for all three clusters are from the west of SETP and they only reflect the transport of air massesappear to originate from the west of SETP (Fig. S4). These differencesThis discrepancy highlights the importance of distinguishing between pure air mass trajectories transport and considering moisture contribution by air masses call for cautionactual moisture sources when interpreting air mass trajectoriesy data.

In contrast, dDuring the summer monsoon season, moisture transport is predominantly transported from the south of SETP, driven by the summer monsoon. The moisture sources and transport pathways for observed in May show someshare similarities with the results forthose of the non-monsoon season, but with notable differences. Compared withSpecifically, the second transport pathway during May (cluster May2) shifts southward toward the AS compared to its counterpart during the non-monsoon (cluster Nov-Apr2), the second transport pathway during May (cluster May2) shows an overall southward shift toward the AS. Similarly, Although thewhile October's air

mass transport ~~pattern~~ direction ~~during October is also similar to that~~mirrors that of ~~during~~ the non-monsoon, the moisture sources and ~~transport~~ pathways ~~for October~~ show ~~similarities~~ greater alignment with ~~the results for~~those of the summer monsoon season, albeit with a slight eastward shift (Figs. 4d and S4d).

Another ~~emerging feature of~~notable aspect of the moisture source distributions is ~~that humidity at SETP is predominantly contributed by air masses over proximal terrestrial regions~~the dominant contribution from proximal terrestrial regions, ~~especially~~ particularly those ~~regions in its~~to the south of SETP (Fig. 4). ~~In contrast, air masses over oceanic regions make a much smaller contribution to humidity at SETP.~~ For ~~instance~~example, the 1% contour ~~of~~ representing moisture contributions ~~by~~ from air parcels over each 1°×1° grid box does not ~~reach~~ extend into oceanic regions during ~~all~~ any of the four seasons. ~~Therefore, moisture uptake of~~This indicates that surface evaporation from oceanic regions~~,~~ such as ~~from~~ the BOB and AS~~, is also very limited~~contributes minimally. Instead, ~~as~~ most of the moisture ~~in air masses~~ originating over these oceanic regions is lost ~~by~~ through precipitation before reaching SETP, and what remains is replenished by evapotranspiration during ~~the~~ transport ~~toward SETP~~over land. This ~~result~~ finding raises an important ~~questions~~ question: do ~~whether~~ the vapor isotop~~ic compositions~~es measured at SETP still ~~preserve~~ reflect the meteorological ~~information~~ conditions at their ocean ~~surface~~ic sources?~~.~~

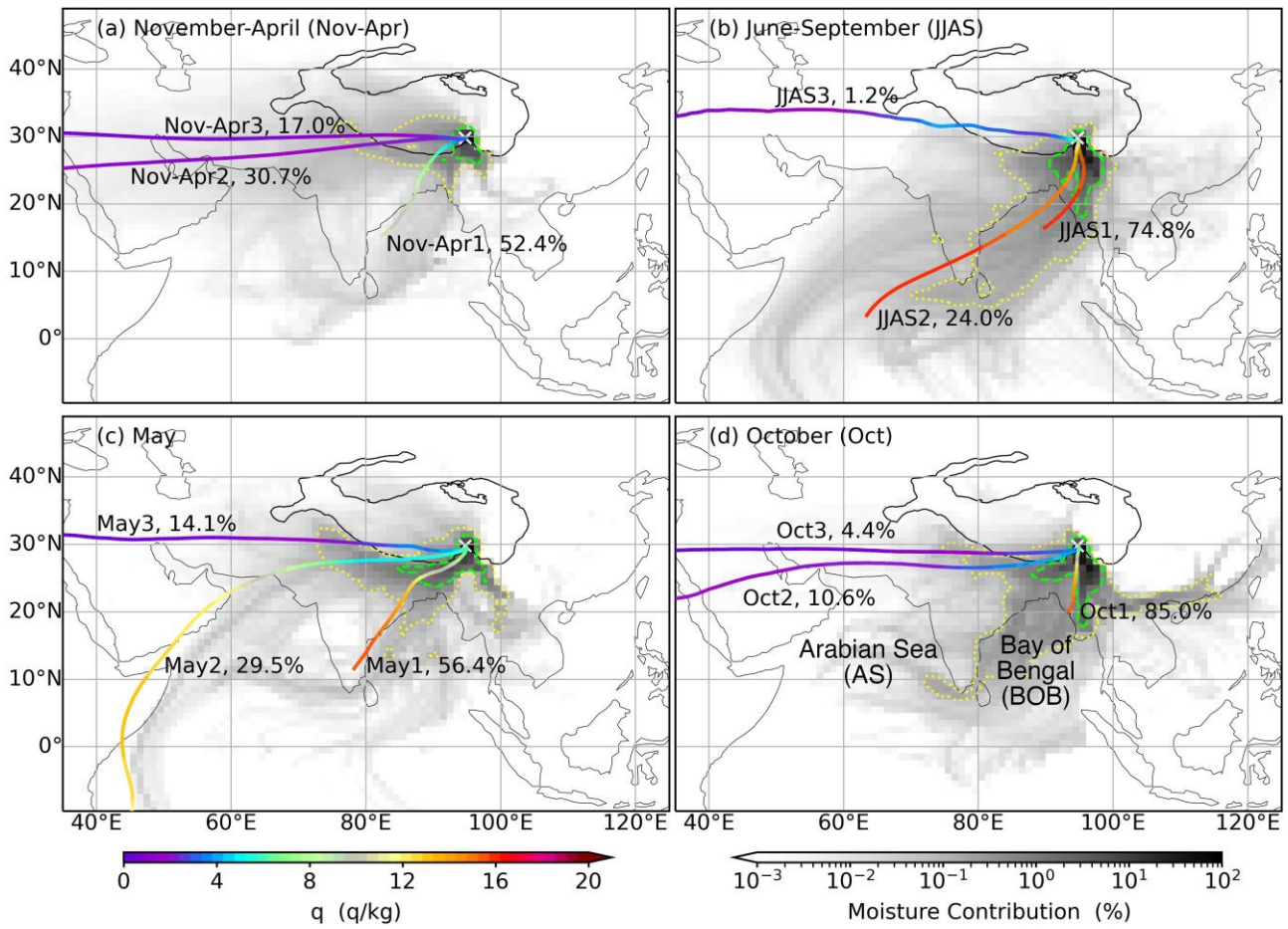
(a) November-April (Nov-Apr)
Nov-Apr3, 17.0%
Nov-Apr2, 30.7%
Nov-Apr1, 52.4%
(b) June-September (JJAS)
JJAS3, 1.2%
JJAS1, 74.8%
JJAS2, 24.0%
(c) May
May3, 14.1%
May2, 29.5%
May1, 56.4%
(d) October (Oct)
Oct3, 4.4%
Oct2, 10.6%
Oct1, 85.0%
Arabian Sea (AS)
Bay of Bengal (BOB)
40°N
30°N
20°N
10°N
0°
40°E
60°E
80°E
100°E
120°E
0
4
8
12
16
20
q (q/kg)
$10^{-3}$
$10^{-2}$
$10^{-1}$
$10^{0}$
$10^{1}$
$10^{2}$
Moisture Contribution (%)

403

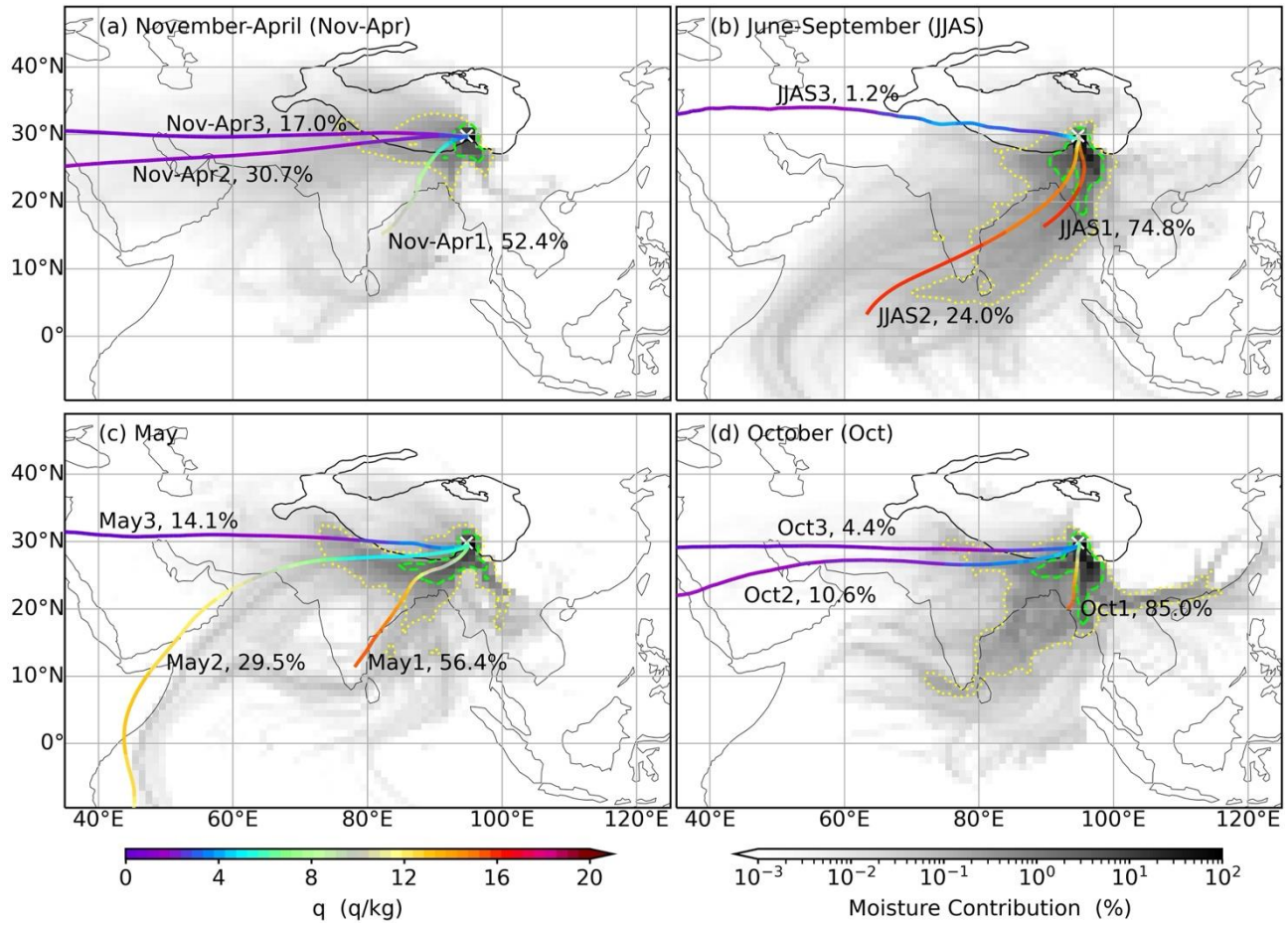


**Figure 4. Moisture sources and transport pathways during different seasons from 2015-2017. (a) spatial distribution of relative contributions of moisture ~~by~~ from all air parcels over ~~all~~ each 1°×1° box (shading) to humidity at the SETP station, along with ~~and~~ specific humidity (*q*) along mean trajectories (weighted by ~~the~~ moisture contributions ~~of air parcels~~) for the non-monsoon season of November-April (Nov-Apr). (b-d) are the same as (a), but for the monsoon season of June-September (JJAS, b), May (c), and October (d), respectivley. The dotted yellow and dashed green contours indicate the moisture contribution at 0.1% and 1%, respectively. The yellow crosses indicate the location of the SETP station. The black solid lines denote the Tibetan Plateau with altitude contour at 3000 m.**

## ~~4 Discussion~~

### ~~4.1~~3.3 Role of ocean surface evaporation conditions at seasonal and intraseasonal time scales

Relationships between ~~vapor~~ *d*-excess and ocean surface evaporation conditions ~~of~~, such as $RH_{SST}$ and SST, ~~are first tested~~were examined using ~~all the~~ data from 2015-2017 (Fig. 5a and Fig. S5a). Results indeed show negative correlations between ~~vapor~~ *d*-excess and $RH_{SST}$ over northern Indian Ocean, ~~especially~~ particularly in the northern parts of AS and BOB (Fig. 5a). ~~Quantitively~~Specifically, the regression slopes ~~of the regression between *d*-excess and $RH_{SST}$~~for this relationship ~~over~~ across the northern Indian Ocean ~~range~~ vary from higher than -0.1‰ $\%^{-1}$ to values below -0.6‰ $\%^{-1}$.

Focusing on specific regions, ~~The regression slopes over~~ the northern BOB (10-22°N and 80-99°E) and the eastern AS (7-20°N and 65-78°E; Fig. 5a) ~~fall~~ exhibited regression slopes within the range (from -0.3‰ $\%^{-1}$ to -0.6‰ $\%^{-1}$) previously reported ~~in previous studies~~ (Uemura et al., 2008; Benetti et al., 2014; Liu et al., 2014; Bonne et al., 2019). For instance, ~~Vapor *d*-excess and~~the regional average $RH_{SST}$ in the eastern AS ~~yields~~ shows an overall regression slope of -0.49‰ $\%^{-1}$ ($r = -0.52$ and $p < 0.01$) ~~for the eastern AS~~ (Fig. ~~S6~~6a) ~~and~~, while the northern BOB has a slope of -0.52‰ $\%^{-1}$ ($r = -0.55$ and $p < 0.01$) ~~for the northern BOB~~ (Fig. ~~S7~~6b). However, upon closer inspection of the *d*-excess- $RH_{SST}$ plots (Fig. 6), it becomes evident that ~~the distribution of data in the *d*-excess and $RH_{SST}$ space suggests a clustering of data~~data points clustered according to ~~that observations during summer months are mainly located in the lower right with high $RH_{SST}$ and low *d*-excess, but in the upper left part of the space for winter months~~ different seasons~~. During each season, there is substantial variability in vapor *d*-excess for a given $RH_{SST}$. These results suggest~~, implying that the apparent negative correlations ~~between *d*-excess and $RH_{SST}$ may mainly~~might primarily ~~arise~~ stem from ~~their~~ oppositeng ~~seasonality~~seasonal trends. Similarly, apparent negative correlations between ~~vapor~~ *d*-excess and SST also emerge over the northern Indian Ocean (Fig. S5a). ~~However~~Yet, both theoretical prediction (Merlivat and Jouzel, 1979) and in-situ observations above the ocean surface (Bonne et al.,

2019; Liu et al., 2014) suggest a positive correlation between ~~vapor~~ *d*-excess and SST. ~~Therefore, we argue~~These discrepancies lead us to speculate that the overall correlations between SETP vapor *d*-excess and surface evaporation conditions over the northern Indian Ocean are ~~mainly a result of their seasonality~~likely driven by seasonal variability ~~and do not hold realistic causal relationships~~.

~~We further examined t~~The relationship between ~~vapor~~ *d*-excess and $RH_{SST}$ was further analyzed by distinguishing between~~for~~ the summer monsoon and non-monsoon seasons~~, respectively~~. During the summer monsoon season, t~~T~~he negative correlation ~~between vapor *d*-excess and $RH_{SST}$ almost totally~~ diminishes significantly, ~~especially during the summer monsoon season when absolute values of~~with correlation coefficients drop ~~to~~ping below 0.3 (Fig. 5b). In contrast, significant~~Stronger~~ correlations present during the non-monsoon season (Fig. 5c), ~~could be~~potentially due to ~~the overall~~ intraseasonal variations ~~that~~ where *d*-excess ~~is the highest during~~peaks in winter and ~~lower~~ decreases at the beginning and ending ~~stages~~of the non-monsoon season (Fig. 1b), ~~which could be~~possibly accompanied ~~with an~~by ~~opposite~~ opposing $RH_{SST}$ trends. ~~Even so~~However, even during the non-monsoon season, ~~the correlations during the non-monsoon still only explain a marginal fraction of~~the explained variance in *d*-excess remains low, at a maximum of ~~(~~10%-16% ~~at maximum~~ over the northern BOB~~)~~. Similarly, correlations with SST over the northern Indian Ocean also become ~~trivial~~ negligible when seasons are considered separately ~~considering the summer monsoon or non-monsoon season~~ (Fig. S5). In summary, vapor *d*-excess at SETP is less likely a conservative tracer of surface evaporation conditions (neither $RH_{SST}$ nor SST) over the northern Indian Ocean. Therefore, ~~it should be cautious when~~ interpreting *d*-excess in meteoric water or paleo archives from the TP as a proxy ~~of~~ for Indian Ocean evaporation conditions ~~over the Indian Ocean~~should be approached with caution.

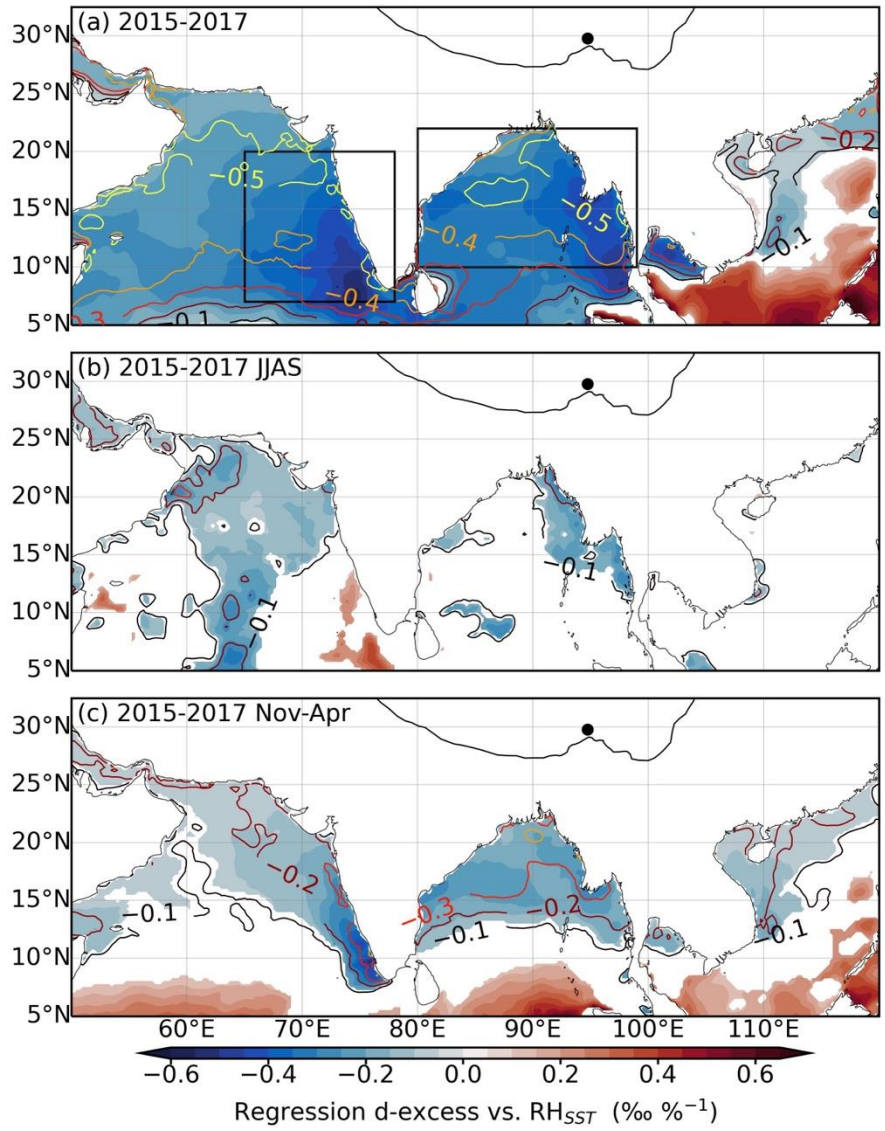


455

456 **Figure 5. Relationships between ~~water~~ vapor *d*-excess and relative humidity scaled to sea surface**

457 **temperature (RH$_{SST}$). (a) regression of ~~vapor~~ *d*-excess against RH$_{SST}$ (shading and only values significant at**

458 **the 95% significance level are shown) and correlation coefficients between them (contours at an interval of**

459 **0.1 and only negative correlations are shown) for all the data from 2015-2017. (b) and (c) are the same as (a)**

460 **but only for the data within the summer monsoon season (JJAS) or the non-monsoon season (Nov-Apr),**

461 **respectively. The black dots indicate the location of the SETP station. The black solid lines denote the Tibetan**

462 **Plateau with altitude contour at 3000 m.**

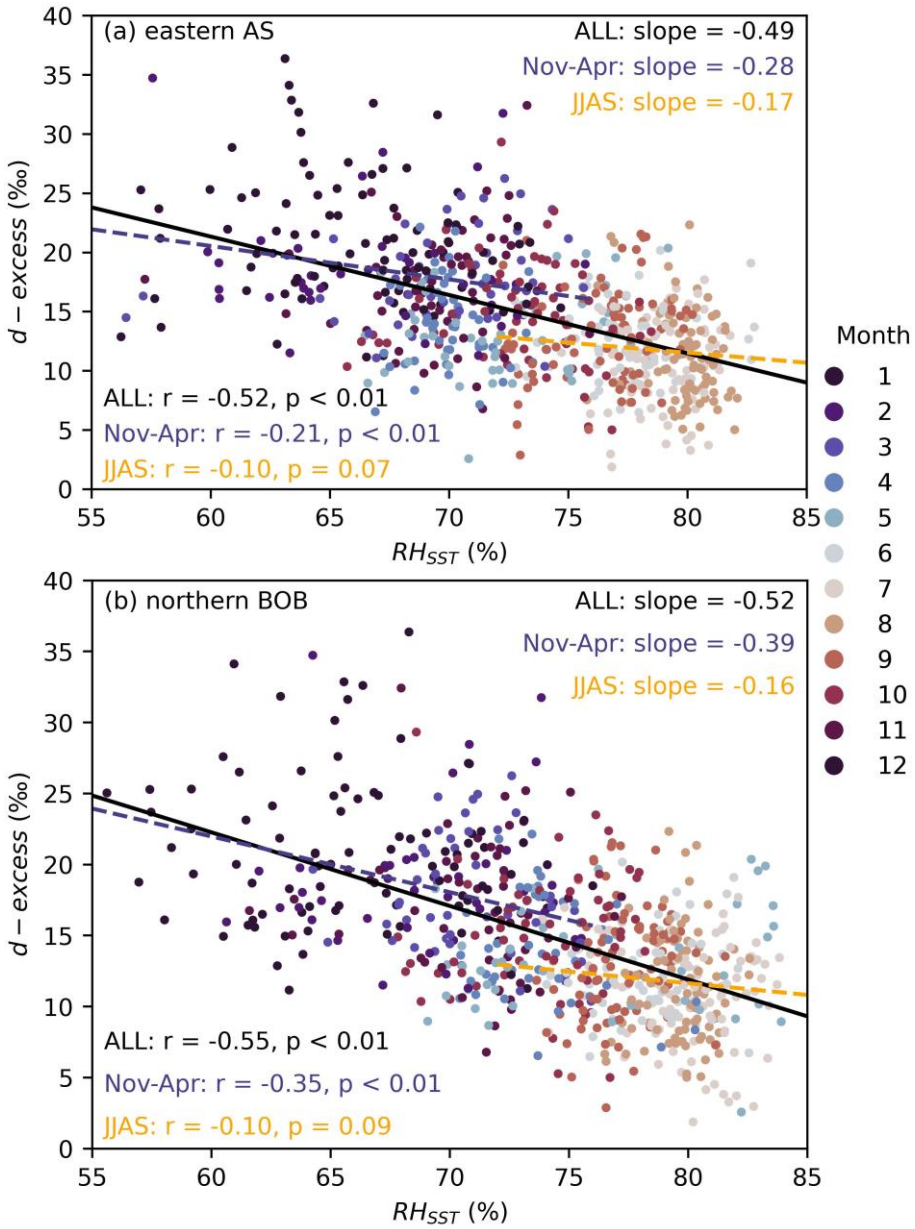


**Figure 6. Relationships between SETP vapor *d*-excess and relative humidity normalized to sea surface temperature ($RH_{SST}$) averaged over (a) eastern Arabian Sea (7-20°N and 65-78°E) and (b) Bay of Bengal (10-22°N and 80-99°E) from 2015-2017. Each data point is color-coded by month. Solid black lines indicate the linear regression between all data points. Dashed orange lines indicate linear regression for data during the non-monsoon season (Nov-Apr) and dashed dark blue lines for data during the summer monsoon (JJAS). The slope (‰ $\%^{-1}$), r, and p values for the three data groups are also shown.**

### ~~4.2~~3.4 Role of dry and cold air intrusion during the non-monsoon season

Both theoretical predictions ~~by~~from the Rayleigh model and observations during the non-monsoon season suggest ~~an increasing trend of~~that ~~vapor~~ *d*-excess increases as ~~when~~ *q* ~~goes to extremely low values~~decreases when *q* reaches extremely low values (Fig. 2). In addition, results for both air mass transport and moisture transport show the dominant role of the westerlies (Figs. S4a and 4a). ~~Therefore~~Based on these evidences, we ~~hypothesize~~ propose that during the non-monsoon season, vapor isotopes are influenced by the mixing of cold and dry air transported by ~~the~~ westerlies from higher altitudes with surface vapor ~~controls vapor isotope compositions during the non-monsoon season~~. Furthermore, s~~S~~urface vapor influenced by recycled moisture from terrestrial evapotranspiration would further elevate ~~vapor~~ *d*-excess at a given *q* (Fig. 3b).

We ~~first did~~performed a composite analysis on moisture sources and transport pathways for the highest (higher than 30‰, and n = 10) and lowest ~~*d*-excess observations~~ (lower than 10‰, and n = 8) *d*-excess observations during the non-monsoon season (Fig. ~~6~~7). ~~For h~~High ~~vapor~~ *d*-excess values~~, moisture is~~ are primarily associated ~~predominantly~~ with moisture transported by westerlies from ~~the~~ regions west of SETP, such as over the TP and northwestern India. In addition, ~~air masses along~~ backward trajectories for these cases ~~are~~ show air masses characterized by extremely low *q*, ~~i.e.~~reaching ~~as low as~~ below 2 g $kg^{-1}$ along the mean trajectories (weighted by ~~the~~ moisture contribution) over the TP (Fig. ~~6a~~7a). Conversely, f~~F~~or low *d*-excess cases, a ~~substantial amount~~significant portion of moisture transport pathways ~~(account for 39.2% by the L1 cluster, Fig. 6b)~~ shifts toward more humid ~~areas~~ regions, including~~of~~ northeast India, Bangladesh, and the BOB, with the L1 cluster accounting for 39.2% (Fig. 7b). This contrasting moisture transport pattern between high and low *d*-excess cases ~~agrees~~ aligns with our hypothesis that ~~the~~ high *d*-excess is associated with dry and cold air transported by ~~the~~ westerlies.

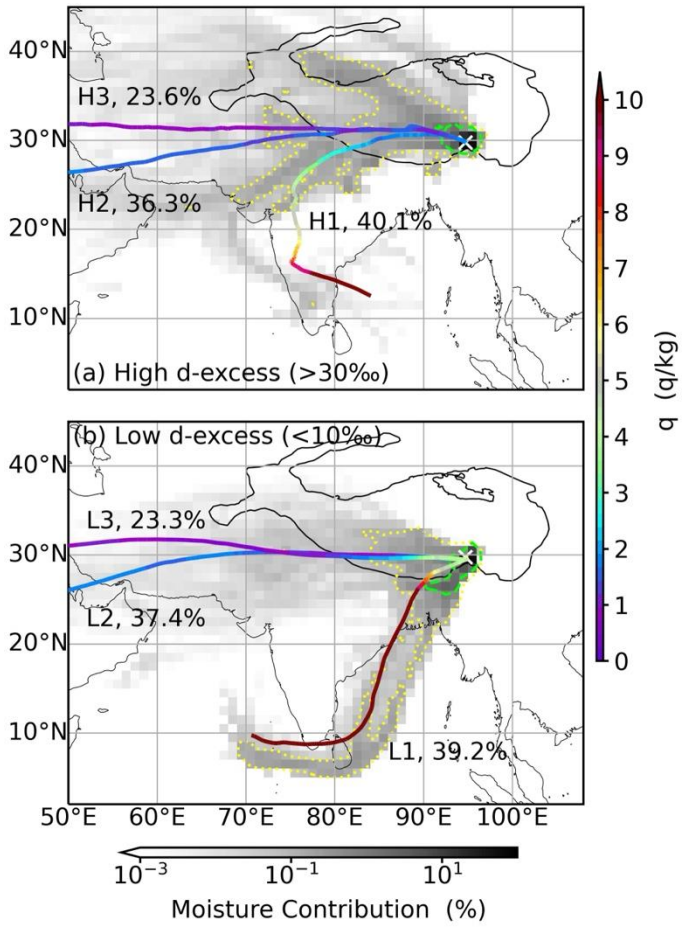


**Figure ~~6~~7. Composite of moisture sources and transport pathways for high and low *d*-excess days during the non-monsoon season of November-April. (a) spatial distribution of relative contribution of moisture ~~by~~ from all air parcels over~~all~~ each 1°×1° box (shading) to humidity at the SETP station, ~~and~~ along with specific humidity (*q*) along mean trajectories (weighted by ~~the~~ moisture contribution ~~of air parcels~~) for *d*-excess values higher than 30‰ during the non-monsoon season (n = 10). (b) is the same as (a) but for *d*-excess lower than 10‰ (n = 8). The yellow crosses indicate the location of the SETP station. The black solid lines denote the Tibetan Plateau with altitude contour at 3000 m.**

~~The relationship between vapor *d*-excess and t~~The ~~intrusion~~ influence of cold and dry air intrusions was~~is~~ further investigated through an analysis of~~tested by~~ relationships ~~among~~ involving~~vapor~~ *d*-excess, local *q*, ~~u~~weighted-mean upstream *q*, weighted-mean upstream air temperature, and weighted-mean upstream air altitude (Fig. ~~7~~8). U~~u~~pstream variables ~~are~~ represent weighted averages~~mean values~~ along the 10-day backward trajectory,

where weights correspond to ~~weighted by~~ the moisture contribution ~~of the air parcel~~ at each time step (~~s~~Section 2.4). The non-monsoon season ~~vapor~~ *d*-excess shows robust negative correlations with both local *q* (r = -0.65, p < 0.01) ~~both at the local scale as well as at~~and upstream *q* (r = ~~-0.65 and~~ -0.67, ~~respectively, and~~ p < 0.01 ~~for both~~). ~~At the same time~~Furthermore, low *q* is associated with air masses ~~with~~ characterized by low temperature~~s~~ and ~~from~~ high altitudes (Figs. ~~7c~~ 8c and ~~7d~~8d)~~. This effect~~, which could also ~~have an~~ impact ~~on vapor~~ $\delta^{18}O$. Indeed, $\delta^{18}O$ during ~~the~~ high *d*-excess cases is lower than ~~$\delta^{18}O$~~ during ~~,~~ ~~the~~ low *d*-excess cases (at a significance level of 95.3%)~~, and~~. ~~the~~ The overall correlation coefficient between $\delta^{18}O$ and *d*-excess during the non-monsoon season is -0.29 (p < 0.01). Notably, c~~C~~orrelations between $\delta^{18}O$ and *q* are weaker compared to those observed for *d*-excess, with local *q* (~~s~~showing r = 0.42 ~~and~~ (p < 0.01) ~~or~~ and upstream *q* (~~s~~showing r = 0.38 ~~and~~ (p < 0.01) ~~are weaker than the correlations between *d*-excess and *q*~~. The relationship between non-monsoon season $\delta^{18}O$ and humidity is mainly expressed as the relationship between $\delta \times q$ and $q$ (r = 0.82 for local *q* and r = 0.90 for upstream *q*).

~~We further analyzed the s~~Spatial ~~distribution of~~ correlations between ~~SETP~~ vapor isotope ~~compositions~~ ($\delta^{18}O$ and *d*-excess) and 2-meter air temperature as well as humidity measured by 2-meter dew point temperature ~~during the non-monsoon season~~also support these findings (Fig. ~~8~~S6). S~~Results show s~~ignificant negative correlations between *d*-excess and dew point temperature ~~at the regional scale~~exist over southeastern TP, northeast India, and northern Bangladesh ~~(Fig. 8a)~~. ~~Correlations with air temperature are generally similar with correlations between *d*-excess and dew point temperature but the most significant correlations are in a smaller region (Fig. 8b).~~ In contrast, ~~correlations between $\delta^{18}O$ and dew point temperature is not as strong as that for *d*-excess (Fig. 8c). Instead, ~~ $\delta^{18}O$ shows ~~stronger~~ significant positive correlations with air temperature over the India subcontinent and ~~the~~ northwestern ~~part of s~~Southeast Asia ~~(Fig. 8d)~~.

As shown in Fig. 3b, ~~E~~extremely high *d*-excess values are predicted at very low *q* levels ~~are predicted in Fig. 3b,. and p~~Previous ~~study~~ studies ~~has~~ have shown that as *q* approaches zero, vapor *d*-excess can approach 7000‰

following the Rayleigh distillation trajectory (Bony et al., 2008), ~~caused by~~a behavior inherent to the definition of ~~the~~ *d*-excess (Dütsch et al., 2017). High ~~vapor~~ *d*-excess values have also been observed in low humidity ~~conditions~~ environments, such as ~~in the~~ polar regions (Bonne et al., 2014; Steen-Larsen et al., 2017) ~~or at~~and high altitudes (Samuels‐Crow et al., 2014; Webster and Heymsfield, 2003; Sayres et al., 2010; Sodemann et al., 2017). Therefore, we infer that the increasing trend of ~~vapor~~ *d*-excess ~~along~~ with decreasing local $q$, upstream $q$, and regional dew point temperature is ~~a result of intensified~~due to enhanced mixing with dry and cold subsiding air transported by ~~the~~ westerlies from high altitudes. Relationships between upstream $q$ and upstream air temperature as well as altitude further support this inference, indicating that low humidity conditions ~~is~~ are associated with the presence of subsiding dry and cold air from high altitudes (Figs. ~~7c~~ 8c and ~~7d~~8d). Therefore, vapor *d*-excess during the non-monsoon not only provides ~~information on~~insights into ~~the~~ specific humidity levels but also indicates the source of humidity.

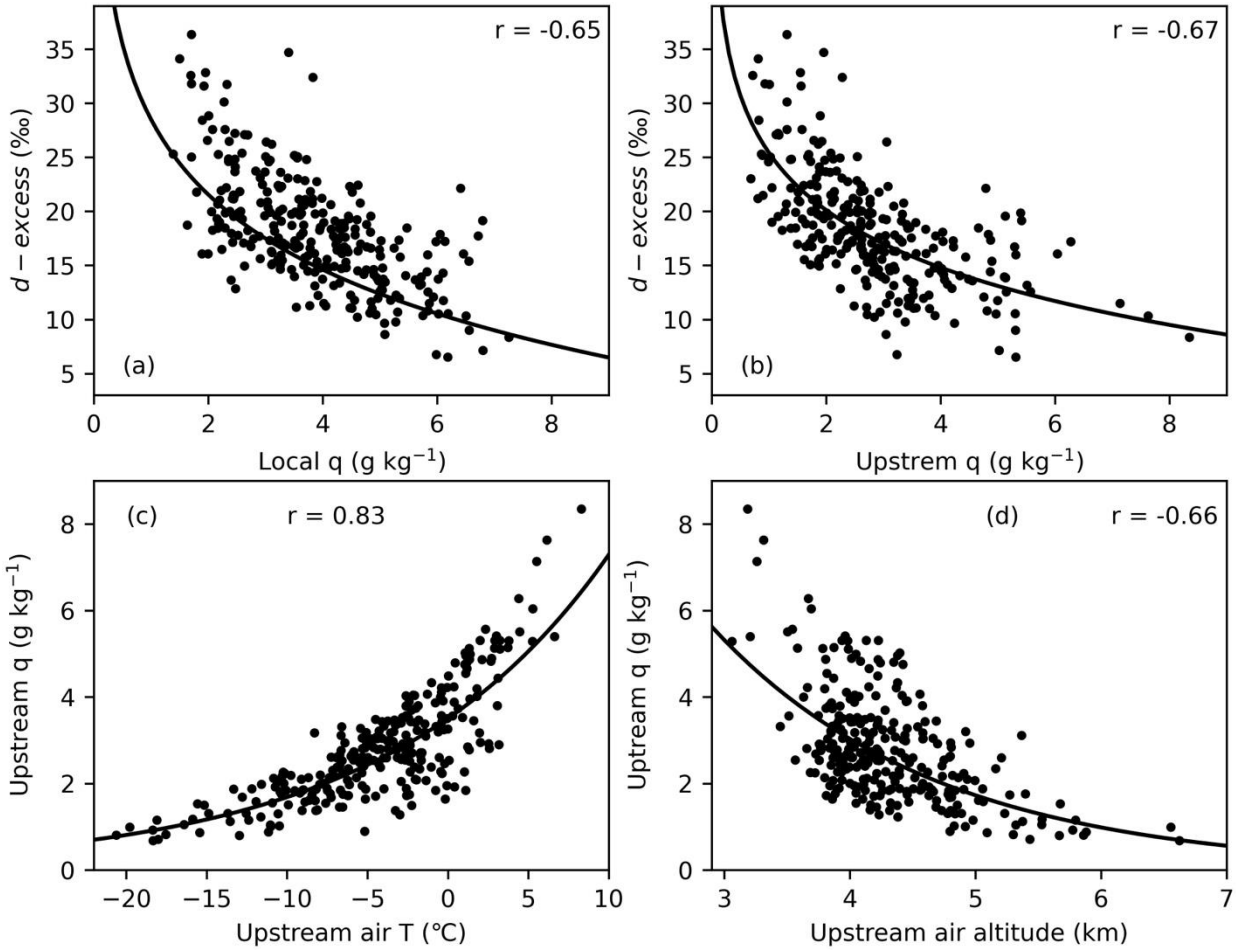


536

537 **Figure ~~7~~8. Relationships among ~~water~~ vapor *d*-excess, local specific humidity (*q*), weighted-mean**

538 **upstream *q*, weighted-mean upstream air temperature (T), and weighted-mean upstream air altitude during**

539 **the non-monsoon season of November-April. (a) scatter plot of *d*-excess against local *q*. (b) scatter plot of *d*-**

540 **excess against upstream weighted-mean *q*. (c) scatter plot of upstream *q* against upstream air T. (d) scatter**

541 **plot of upstream *q* against upstream air altitude. All the upstream variables are mean values along backward**

542 **trajectories weighted by the moisture contribution of air parcels. The solid curves indicate the log regression**

543 **between the respective variables with the correlation coefficients indicated by the numbers.**

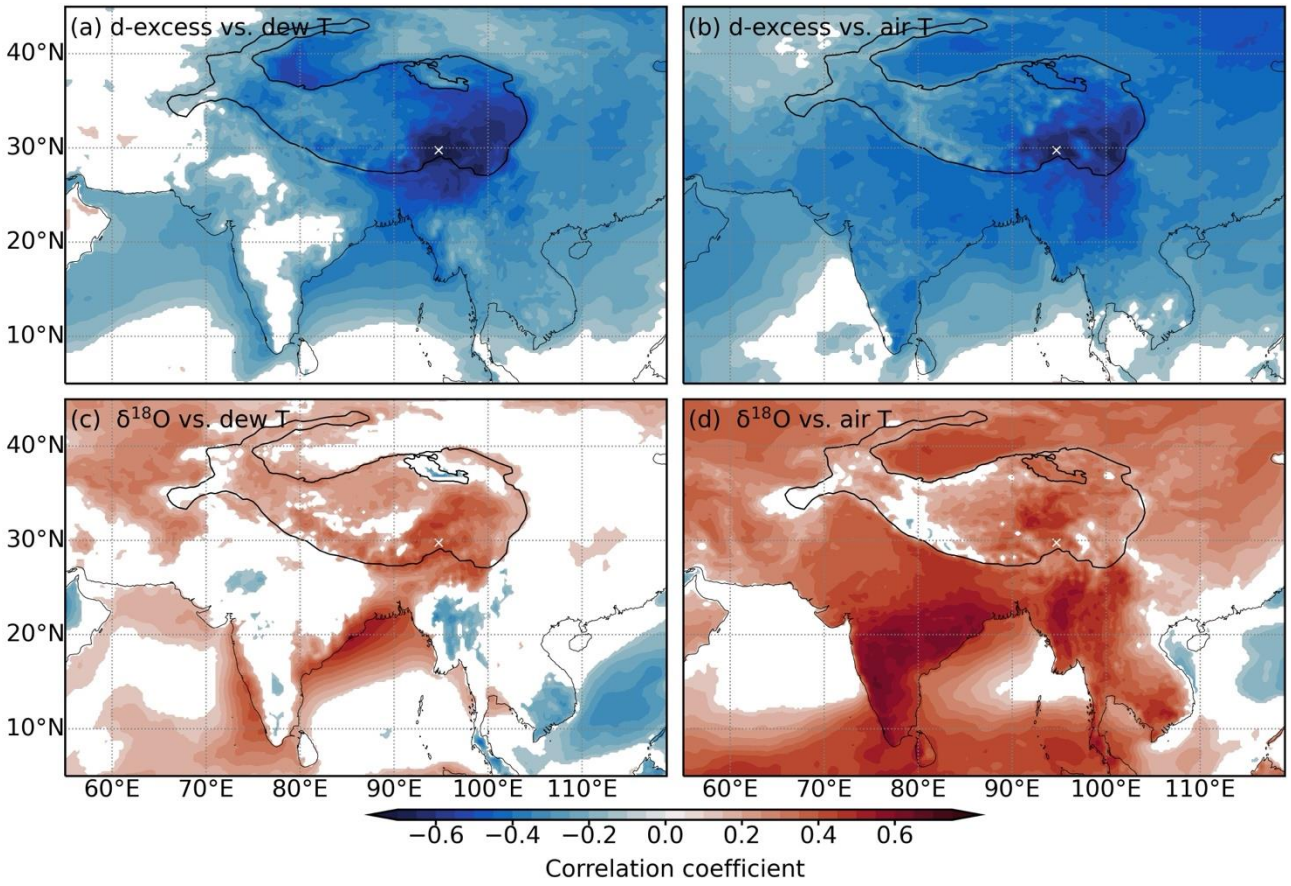


~~**Figure 8. Spatial distribution of correlation coefficients among water vapor isotope compositions, dew point temperature, and air temperature during the non-monsoon season of November-April. (a) spatial distribution of correlation coefficients between SETP vapor *d*-excess and 2-meter dew point temperature. (b) the same as (a) but with 2-meter air temperature. (c) the same as (a) but between $\delta^{18}O$ and 2-meter dew point temperature. (d) the same as (c) but with 2-meter air temperature. Only values significant at the 95% significance level are shown. The white crosses indicate the location of the SETP station. The black solid lines denote the Tibetan Plateau with altitude contour at 3000 m.**~~

### ~~4.3~~3.5 Role of rain-vapor interaction during the summer monsoon season

~~Different from~~In contrast to the significant dependence of ~~vapor~~ *d*-excess on *q*~~specific humidity~~ during the non-monsoon season, vapor *d*-excess ~~is not correlated~~shows no correlation with *q*~~specific humidity~~ ($r = 0.04$ ~~and~~, $p = 0.51$) during the summer monsoon season. The behavior of $\delta^{18}O$ ~~is~~ also ~~distinct during~~differs between the two

seasons (Fig. 3). During the ~~Distribution of~~s ~~s~~ummer monsoon season, ~~observations in the~~ $\delta^{18}O$-*q* plots ~~space~~ below the Rayleigh curve, ~~suggests~~ indicating that the vapor has undergone a ~~certain~~ degree of rain-vapor interaction ~~by~~ ~~rain~~due to evaporation (Fig. 3a). ~~On the other hand, p~~Partial rain evaporation in an unsaturated atmospheric environment ~~is associated~~leads to ~~with~~ kinetic fractionation, which decreases ~~the~~ *d*-excess values ~~of the~~in raindrops ~~but increases the~~while increasing *d*-excess in the~~of~~ surrounding vapor (Risi et al., 2008b). This effect of rain-vapor interaction on vapor isotope ~~compositions~~ has been suggested as a ~~major process responsible for~~primary mechanism driving the amount effect in ~~the~~ tropic~~s~~al regions (Risi et al., 2008a; Kurita et al., 2011; Bowen et al., 2019; Galewsky et al., 2016). Therefore, we hypothesize that vapor isotope ~~compositions~~ during the summer monsoon season at SETP are ~~controlled~~ influenced by the degree of rain-vapor interaction.

The first evidence supporting this hypothesis is ~~that~~the significant correlation between ~~vapor~~ $\delta^{18}O$ ~~is significantly correlated with~~and *d*-excess during the summer monsoon season ($r = -0.55$ ~~and~~, $p < 0.01$~~,~~; Fig. 9a). In addition, there is a trend ~~that~~where ~~vapor~~ $\delta^{18}O$ and *d*-excess ~~are less correlated~~exhibit weaker correlations when $\delta^{18}O$ ~~is high and the opposite for low $\delta^{18}O$~~ levels are high, and stronger correlations when $\delta^{18}O$ levels are low (Figs. 9a and ~~S8~~S7). ~~If there is no rain, rain-vapor interaction is not possible. Therefore~~To explore this further, we ~~flitted data during days when the~~categorized days with daily precipitation ~~amount is not less than~~of at least 2 mm as "rainy days" and ~~days~~ those with ~~precipitation~~ less than 2 mm as ~~no rain occurs locally (~~"non-rainy days"~~)~~. This distinction is based on the premise that rain-vapor interaction cannot occur in the absence of rainfall. The analysis reveals that ~~Vapor~~ $\delta^{18}O$ during rainy days is significantly ~~higher~~ lower than that during non-rainy days, ~~and~~while *d*-excess show the opposite trend ~~applies for *d*-excess~~ ($p < 0.01$ for both $\delta^{18}O$ and *d*-excess~~) (~~; Figs. 9b and 9c). Furthermore, t~~T~~he correlation between ~~vapor~~ $\delta^{18}O$ and *d*-excess becomes stronger ~~during~~ on rainy days ~~becomes stronger~~ ($r = -0.69$ ~~and~~, $p < 0.01$~~). However, vapor $\delta^{18}O$ is still negatively correlated with *d*-excess during~~, though a weaker negative correlation persists even on non-rainy days ($r = -0.40$ ~~and~~, $p < 0.01$). Even ~~if~~ when applying a stricter

threshold of 0 mm for ~~daily precipitation amount is used for flittering~~ non-rainy days, ~~there is still a~~the ~~significant~~ negative correlation between ~~vapor~~ $\delta^{18}O$ and *d*-excess remains significant (r = -0.37 ~~and~~, p < 0.01). ~~In addition~~Moreover, correlations with local precipitation amount are weak ~~both~~ for both $\delta^{18}O$ (r = -0.31 ~~and~~, p < 0.01) and *d*-excess (r = 0.26 ~~and~~, p < 0.01). ~~Therefore, we further~~These findings lead us to infer that vapor isotopes during the summer monsoon season at SETP are influenced not only by local ~~the effect of~~ rain-vapor interactions ~~is not only from the local scale~~ but also ~~inherit~~bys the history of rain-vapor interactions ~~before vapor has been transported to SETP~~that occurred before the vapor reached the region.

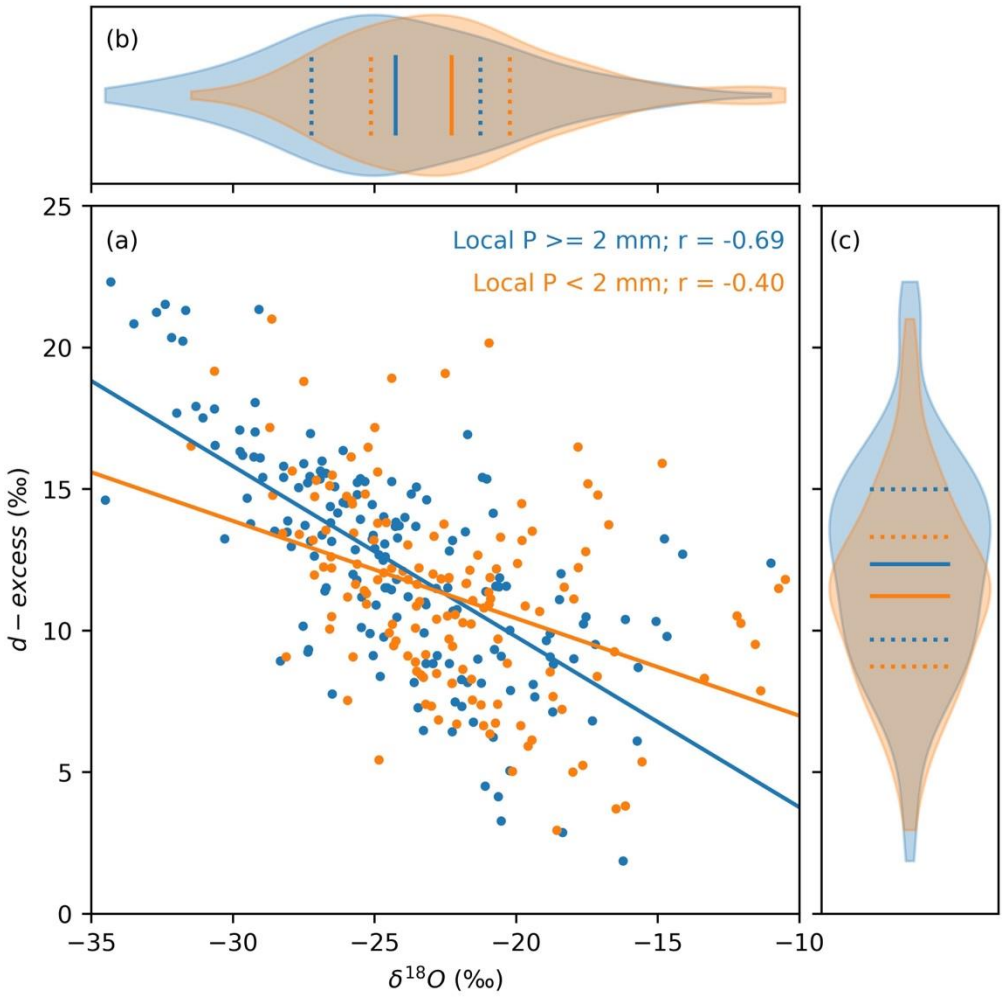


**Figure 9. Relationships between SETP vapor *d*-excess and $\delta^{18}O$ during the summer monsoon season. (a) scatter plot of *d*-excess against $\delta^{18}O$ and linear regression lines between them. (b) distribution of $\delta^{18}O$ values with the dashed lines indicate values at the lower and upper quartiles and the solid lines indicate the mean**

**values. (c) is the same as (b) but for *d*-excess. Orange colors indicate data observed during daily precipitation amount less than 2 mm and blue colors indicate data observed during days with precipitation amount not less than 2 mm. The r values for both lines are indicated in (a) and both of them are significant at the 0.01 level.**

~~If there is a larger amount of rainfall, the effect of rain-vapor interaction on atmospheric humidity would be stronger. Therefore~~To further investigate the role of rain-vapor interactions, we use total precipitation amount ($P_{acc}$) as ~~a measure of~~an indicator of rain-vapor interaction, considering the cumulative effect over several days preceding sampling. ~~To account for the history during moisture transport, the total precipitation amount during several days before sampling is considered. We have tested~~Our analysis examined correlations ~~the relationships~~ between vapor isotope ~~compositions~~ ($\delta^{18}O$ and *d*-excess) and $P_{acc}$ ~~over~~ for periods ranging from 1-10 days prior to sampling (Figs. ~~S9~~ S8 and ~~S10~~S9). Vapor *d*-excess reaches an optimal correlation with $P_{acc}$ when ~~the total precipitation amount during~~considering 3 days before sampling ($P_{acc\_3d}$) ~~is considered~~. Vapor $\delta^{18}O$ shows a slightly longer memory and reaches an optimal correlation ~~with $P_{acc}$ when the total precipitation amount during~~around 5-6 days before sampling ~~is considered~~. Fig. 10 shows the spatial distribution of these correlations, ~~between vapor isotope compositions ($\delta^{18}O$ and *d*-excess) and $P_{acc\_3d}$. Vapor~~where *d*-excess ~~shows significant positive correlations~~positively correlates with $P_{acc\_3d}$ ~~in the region surrounding SETP with a spatial scale of~~across a ~5°×5° region surrounding SETP and ~~the positive correlation~~ extend~~s~~ing southwestward to the ~~foothill of the~~ Himalayas (Fig. 10a). In contrast, ~~vapor~~ $\delta^{18}O$ shows significant negative correlations ~~with $P_{acc\_3d}$~~ in similar regions (Fig. 10b). Interestingly, even~~For~~ on non-rainy days, ~~vapor $\delta^{18}O$ and *d*-excess still show~~ significant regional-scale correlations ~~with $P_{acc\_3d}$ at regional scale~~persist, albeit ~~with~~ weaker ~~correlation levels~~ and with a smaller spatial extent (Fig. ~~S11~~S10).

These ~~significant correlations among vapor $\delta^{18}O$, *d*-excess, and $P_{acc\_3d}$~~findings provide further evidence for understanding ~~processes that are responsible for~~the mechanisms driving the amount effect. The negative correlation

between $\delta^{18}O$ and $P_{acc\_3d}$ ~~has~~ also been observed in precipitation and can be ~~interpreted in terms of~~attributed to either continuous rainout (Scholl et al., 2009; Vuille et al., 2003; Ruan et al., 2019) or ~~the effect of~~ rain-vapor interactions (Lawrence et al., 2004; Risi et al., 2008a; Kurita et al., 2011; Worden et al., 2007). ~~Although~~ While continuous rainout, explained by the Rayleigh distillation model, ~~with increased rainfall amount can explain~~accounts for the decreasing trend of $\delta^{18}O$ with increased rainfall ~~by the Rayleigh distillation model~~, *d*-excess ~~stays~~ remains ~~at a~~ relatively stable ~~level when~~unless specific humidity ~~is not very low~~drops to very low levels (~~above~~ ~4 g $kg^{-1}$ in Fig. 3b for example). ~~Therefore, t~~The positive correlation between vapor *d*-excess and $P_{acc\_3d}$ provides an additional constraint, suggesting that the amount effect is not ~~simply~~ solely a result of rainout but ~~rain-vapor interaction plays an important role in altering lower tropospheric isotope compositions~~also involves rain-vapor interactions, which significantly influence vapor isotopes in the lower troposphere.

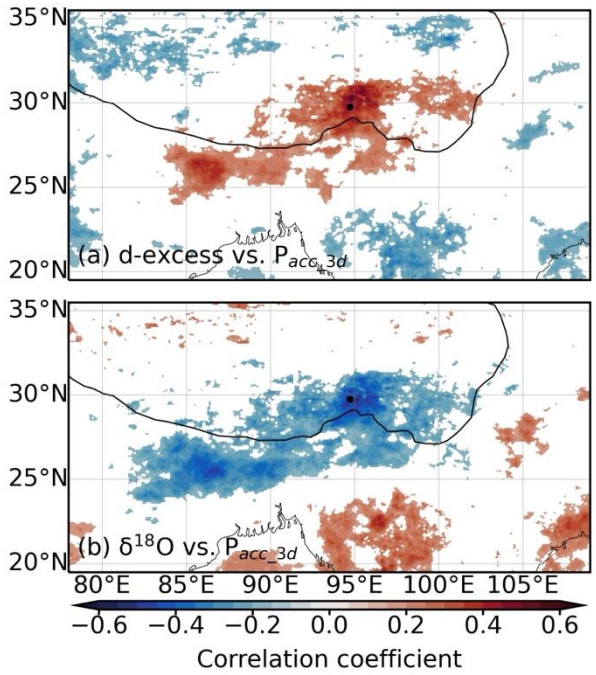


**Figure 10. Relationships between vapor isotop~~e compositions~~s for rainy days (local daily precipitation amount not less than 2 mm) and total precipitation amount at the regional scale during the summer monsoon season. (a) spatial distribution of correlation coefficients between ~~vapor~~ *d*-excess and total precipitation amount during 3 days prior sampling ($P_{acc\_3d}$). (b) is the same as (a) but for $\delta^{18}O$. Only values significant at**

**the 95% significance level are shown. The black dots indicate the location of the SETP station. The black solid lines denote the Tibetan Plateau with altitude contour at 3000 m.**

## 4 Implications for interpreting TP ice core isotope data

### ~~4.4 An alternative interpretation for the high *d*-excess in high-altitude TP ice cores~~

Interpret~~ations~~ing ~~of~~ *d*-excess in meteoric water and ice cores on the TP ~~are~~ is complicated by evaporation conditions over the northern Indian Ocean ($RH_{SST}$ and SST) and continental recycling (Shao et al., 2021; Zhao et al., 2012; Joswiak et al., 2013; Pang et al., 2012; An et al., 2017). Attempts have been made to establish ~~a~~ relationships between vapor *d*-excess and $RH_{STT}$ (Chen et al., 2024; Liu et al., 2024) as well as between ice core *d*-excess and $RH_{STT}$ (Shao et al., 2021) or SST (Zhao et al., 2012). Based on ~~relationships between vapor *d*-excess and surface evaporation conditions discussed above~~results in Section 3.3, however, the apparent relationships are ~~mainly~~ primarily a result of similarities in the seasonality of these variables.

Furthermore, the direct contribution of oceanic ~~water~~ vapor ~~contained in air masses over oceanic regions~~ to humidity at SETP is very limited (Fig. 4), ~~which implies~~implying an even smaller contribution ~~that the contribution to humidity~~ over the TP since SETP~~is further decreased than at SETP as it~~ is at the forefront of moisture transport toward TP (Fig. S1). The dominant terrestrial origin indicates ~~that the moisture has undergone a certain degree of~~significant continental recycling. Terrestrial processes such as transpiration and evaporation introduce isotopically enriched moisture and high *d*-excess signatures, respectively. Mixing with terrestrial sources is also reflected in the relationship between vapor isotope ~~compositions~~ and *q* (Fig. 3). ~~The degree of continental recycling also alters vapor isotope compositions that transpiration introduces isotopically enriched moisture and evaporation introduces moisture with high *d*-excess. Seasonally changing isotope signatures in precipitation and ice cores as well as variations at longer timescales~~Seasonal changes and long-term variations in precipitation and ice core isotopes have

been interpreted as shifts in moisture source ~~shift~~ between recycled terrestrial moisture ~~over terrestrial regions~~ and oceanic ~~moisture~~ sources or their relative contributions (An et al., 2017; Yang and Yao, 2020). ~~A further inference of this process is that the o~~Oceanic moisture is ~~brought by~~typically associated with the summer monsoon, while ~~the~~ westerlies bring moisture from continental recycling or even the Mediterranean Sea~~,~~. Water isotope signatures on the TP were thought to reflect this~~and therefore water isotope signatures reflect the~~ interplay between the summer monsoon and westerlies (Joswiak et al., 2013; Pang et al., 2012; Tian et al., 2007). ~~Although our results also indicate~~Despite seasonally shifting moisture sources, continental recycling prevails throughout the year (Fig. 4). ~~Besides focusing on moisture sources at the Earth surface, we provide a~~Our~~n~~ alternative perspective ~~to~~ explains ~~the~~ high *d*-excess induced by ~~the~~ westerlies as dry and cold air intrusions rather than surface evaporation or evapotranspiration. ~~In this circumstance, the interpretation of~~While the interplay between the summer monsoon and westerlies ~~is still~~remains valid, but we emphasize changes in air mass ~~property~~ properties driven by ~~the~~ different circulation systems.

The proposed alternative interpretation could also help ~~understand~~explain the abnormally high *d*-excess in high-altitude ice cores mentioned in the Introduction. ~~the increasing trend of precipitation and river water isotope observations toward ice cores at higher altitudes on the TP~~ This is because~~as~~ specific humidity ~~is very low~~ at these ice core sites is extremely low, and prolonged interaction with cold and dry air may further modify snow isotope compositions (Ma et al., 2024; Wahl et al., 2022). In addition, intense rain-vapor interactions during the summer monsoon ~~is~~ represent another potential source of ~~higher~~ elevated~~vapor~~ *d*-excess (~~section~~ Section ~~4.3~~3.5). When this high~~Higher vapor~~ *d*-excess vapor contributes to subsequent precipitation, its signal ~~could~~ can be inherited in ~~subsequent~~ the resulting precipitation ~~when it feeds the precipitation~~ (Risi et al., 2008b). However, a clear relationship between TP precipitation *d*-excess and monsoon convection has ~~not been~~yet to be established ~~yet~~, partly due to ~~less~~ limited attention ~~has been~~ paid to *d*-excess in previous studies. On the other hand, local raindrop

evaporation may counteract this effect by reducing raindrop *d*-excess values.~~Nevertheless, summer monsoon rainfall *d*-excess observed on the TP is generally between 0-10‰ (Tian et al., 2001). Raindrop evaporation at upstream increases vapor *d*-excess and therefore could cause elevated *d*-excess in downstream rainfall. On the contrary, this effect can be compensated by on-site raindrop evaporation as it lowers raindrop *d*-excess values.~~ The overall positive correlation between precipitation *d*-excess and altitude ~~in~~ across Asia has ~~been~~ sometimes been ~~interpreted~~attributed to ~~as~~ stronger evaporation at lower altitudes (Bershaw, 2018). For snowfall on glaciers, however, evaporation ~~is less likely~~ for falling snowflakes is less likely due to cold temperatures and the short distance between the cloud base and the glacier surface. Therefore, elevated vapor *d*-excess signals caused by accumulated rain-vapor interactions at upstream associated with monsoon convection could be ~~another source for~~a possible source of the high *d*-excess in ice cores.

## 5 Conclusions

We present a three-year-long daily near-surface ~~water~~ vapor isotope ~~compositions~~ dataset observed at the ~~South East TP~~SETP station, which is at the major channel for moisture entering the TP. ~~Our vapor isotope compositions~~The paired measurements of vapor isotopes and~~with~~ specific humidity ~~reflect~~ reveal distinct moisture sources and dynamics between ~~the~~ non-monsoon and summer monsoon seasons, consistent with findings from Lagrangian moisture diagnostic~~ results~~. Despite significant negative correlations between~~ vapor~~ *d*-excess and relative humidity scaled to sea surface temperature ~~existing~~ over the northern Indian Ocean when ~~data for~~ all seasons are considered, ~~such correlations with oceanic surface evaporation conditions largely disappear when separately considering each season~~these correlations weaken or even disappear when analyzed within individual seasons. This ~~result questions~~finding challenges the ~~early~~ earlier interpretation of TP *d*-excess as indicator of oceanic evaporation conditions and guarantees new interpretations in the future.

During the non-monsoon season, vapor *d*-excess is ~~mainly~~primarily influenced by specific humidity ~~both~~ at both ~~the~~ local ~~scale~~ and upstream scales. ~~Highly~~ Air that has undergone significant dehydration, situated~~ed air~~ at the lower end of the Rayleigh distillation, is expected to have extremely high *d*-excess values. ~~Air mass~~Backward trajectory analyses and moisture source diagnostics ~~suggest~~ reveal that the intrusion of cold and dry air ~~intrusion~~ driven by ~~the~~ westerlies during the non-monsoon season leads to the increasing trend ~~of~~ in ~~vapor~~ *d*-excess ~~along with decreasing~~as specific humidity decreases. This process also contributes to a weak negative correlation between ~~vapor~~ *d*-excess and $\delta^{18}O$. Furthermore, ~~vapor~~ $\delta^{18}O$ primarily reflects mixing processes ~~with~~ involving a relatively enriched moist end-member compared ~~with~~ to the summer monsoon season. These new insights into vapor *d*-excess ~~on~~ during the non-monsoon season ~~vapor *d*-excess~~ provide~~s~~ an alternative ~~way~~ framework for ~~to~~ interpreting the high *d*-excess in high-altitude TP ice cores.

During the summer monsoon season, rain evaporation ~~is~~ emerges as the dominant process ~~determining~~ shaping ~~water~~ vapor isotope compositions. First, ~~vapor~~ $\delta^{18}O$ systematically shifts below the Rayleigh distillation curve, aligning with predictions of ~~falling in the region predicted by~~ "super-Rayleigh" distillation ~~driven~~ caused by partial rain evaporation. Second, ~~vapor~~ $\delta^{18}O$ is anti-correlated with *d*-excess, pointing to ~~an origin of depleted vapor by~~ kinetic fractionation as a source of depleted vapor, which ~~is not likely simply a result of~~cannot be attributed solely to rainout. Third, at the regional scale, ~~vapor~~ $\delta^{18}O$ ~~is~~ shows significant~~ly~~ negative~~ly correlated~~ correlations with total precipitation amount ~~at the regional scale~~, ~~but~~ while ~~vapor~~ *d*-excess positively correlates with total precipitation amount. These ~~results~~ findings ~~help us~~enhance our understanding of ~~the dynamics of~~ atmospheric humidity dynamics and ~~also~~ help disentangle the different effects of rainout and rain-vapor interactions in the context of the amount effect.

This study reveals distinct moisture sources and dynamics between non-monsoon and monsoon seasons over the southeastern Tibetan Plateau. These findings will aid in interpreting $\delta^{18}O$ and *d*-excess records from Tibetan

Plateau glaciers, offering refined insights into past hydroclimatic conditions and challenging assumptions linking ice core isotopes to oceanic evaporation alone. ~~Overall, the new findings from the study reveal different moisture sources and dynamics between the non-monsoon and monsoon seasons over the southeastern TP. The findings will also help the interpretation of ice core $\delta^{18}O$ and *d*-excess records derived from glaciers on the TP.~~

## Competing interests

The authors declare that they have no conflict of interest.

## Acknowledgements

We thank the editors and the referees for their comments and suggesetions. This research ~~is~~ was supported by the National Key R&D Program of China (Grant 2024YFF0807901), the National Natural Science Foundation of China (Grant 42371144), the Yunnan Fundamental Research Projects (Grant 202301AT070183), and the funding of Donglu Talent Young Scholar from the Yunnan University and support for young scholars from the Double First-Class Initiative for Ecological Disciplines of the Yunnan University. We would like to thank the staff at the South-East Tibetan Plateau Station for integrated observation and research of alpine environment for their help in collecting water samples and for sharing the meteorological data at the station.

## Data availability

The NOAA ARL provided the HYSPLIT model and the GDAS data (https://www.ready.noaa.gov/HYSPLIT.php). The Copernicus Climate Change Service provided the ERA5 data (https://doi.org/10.24381/cds.adbb2d47 and https://doi.org/10.24381/cds.f17050d7). The GPM data are available through GES DISC (https://doi.org/10.5067/GPM/IMERG/3B-HH/07). Local meteorological data at the SETP station are provided by National Tibetan Plateau / Third Pole Environment Data Center

(https://dx.doi.org/10.11888/AtmosphericPhysics.tpe.68.db). The observation data at the SETP station have been uploaded to Figshare and will be made publicly available after publication (10.6084/m9.figshare.27302871).

## Author contributions

**Zhongyin Cai**: Conceptualization, methodology, investigation, formal analysis, funding acquisition, writing-original draft, writing-review & editing; **Rong Li**: Investigation, data curation, writing-review & editing; **Cheng Wang**: Validation; **Qiukai Mao**: Investigation, **Lide Tian**: Resources, project administration, funding acquisition.

## References


Aemisegger, F., Pfahl, S., Sodemann, H., Lehner, I., Seneviratne, S. I., and Wernli, H.: Deuterium excess as a proxy for continental moisture recycling and plant transpiration, Atmos. Chem. Phys., 14, 4029-4054, 10.5194/acp-14-4029-2014, 2014.

An, W., Hou, S., Zhang, Q., Zhang, W., Wu, S., Xu, H., Pang, H., Wang, Y., and Liu, Y.: Enhanced Recent Local Moisture Recycling on the Northwestern Tibetan Plateau Deduced From Ice Core Deuterium Excess Records, J. Geophys. Res., 122, 12,541-512,556, 10.1002/2017jd027235, 2017.

Araguás-Araguás, L., Fröehlich, K., and Rozanski, K.: Stable isotope composition of precipitation over southeast Asia, J. Geophys. Res., 103, 28721-28742, 1998.

Benetti, M., Reverdin, G., Pierre, C., Merlivat, L., Risi, C., Steen-Larsen, H. C., and Vimeux, F.: Deuterium excess in marine water vapor: Dependency on relative humidity and surface wind speed during evaporation, J. Geophys. Res., 119, 584-593, 2014.

Bershaw, J.: Controls on Deuterium Excess across Asia, Geosciences, 8, 257, 10.3390/geosciences8070257, 2018.

Bonne, J.-L., Behrens, M., Meyer, H., Kipfstuhl, S., Rabe, B., Schönicke, L., Steen-Larsen, H. C., and Werner, M.: Resolving the controls of water vapour isotopes in the Atlantic sector, Nature Communications, 10, 1632, 10.1038/s41467-019-09242-6, 2019.

Bonne, J. L., Masson-Delmotte, V., Cattani, O., Delmotte, M., Risi, C., Sodemann, H., and Steen-Larsen, H. C.: The isotopic composition of water vapour and precipitation in Ivittuut, southern Greenland, Atmos. Chem. Phys., 14, 4419-4439, 10.5194/acp-14-4419-2014, 2014.

Bony, S., Risi, C., and Vimeux, F.: Influence of convective processes on the isotopic composition ($\delta^{18}O$ and $\delta D$) of precipitation and water vapor in the tropics: 1. Radiative-convective equilibrium and Tropical Ocean–Global Atmosphere–Coupled Ocean-Atmosphere Response Experiment (TOGA-COARE) simulations, J. Geophys. Res., 113, D19305, 10.1029/2008JD009942, 2008.

Bowen, G. J. and Wilkinson, B.: Spatial distribution of $\delta^{18}O$ in meteoric precipitation, Geology, 30, 315, 10.1130/0091-7613(2002)030<0315:sdooim>2.0.co;2, 2002.

765 Bowen, G. J., Cai, Z., Fiorella, R. P., and Putman, A.: Isotopes in the Water Cycle: Regional- to Global-Scale
766 Patterns and Applications, Annu. Rev. Earth Planet. Sci., 47, 453-479, 10.1146/annurev-earth-053018-060220,
767 2019.
768 Breitenbach, S. F. M., Adkins, J. F., Meyer, H., Marwan, N., Kumar, K. K., and Haug, G. H.: Strong influence of
769 water vapor source dynamics on stable isotopes in precipitation observed in Southern Meghalaya, NE India, Earth
770 Planet. Sci. Lett., 292, 212-220, 10.1016/j.epsl.2010.01.038, 2010.
771 Cai, Z. and Tian, L.: Atmospheric controls on seasonal and interannual variations in the precipitation isotope
772 in the East Asian Monsoon region, J. Climate, 29, 1339-1352, 10.1175/JCLI-D-15-0363.1, 2016.
773 Cai, Z. and Tian, L.: What causes the post-monsoon $^{18}O$ depletion over Bay of Bengal head and beyond?,
774 Geophys. Res. Lett., 47, e2020GL086985, 10.1029/2020gl086985, 2020.
775 Cai, Z., Tian, L., and Bowen, G. J.: ENSO variability reflected in precipitation oxygen isotopes across the Asian
776 Summer Monsoon region, Earth Planet. Sci. Lett., 475, 25-33, 10.1016/j.epsl.2017.06.035, 2017.
777 Cai, Z., Tian, L., and Bowen, G. J.: Spatial-seasonal patterns reveal large-scale atmospheric controls on Asian
778 Monsoon precipitation water isotope ratios, Earth Planet. Sci. Lett., 503, 158-169, 10.1016/j.epsl.2018.09.028, 2018.
779 Cao, R., Huang, H., Wu, G., Han, D., Jiang, Z., Di, K., and Hu, Z.: Spatiotemporal variations in the ratio of
780 transpiration to evapotranspiration and its controlling factors across terrestrial biomes, Agr. Forest Meteorol., 321,
781 108984, 10.1016/j.agrformet.2022.108984, 2022.
782 Chen, M., Gao, J., Luo, L., Zhao, A., Niu, X., Yu, W., Liu, Y., and Chen, G.: Temporal variations of stable isotopic
783 compositions in atmospheric water vapor on the Southeastern Tibetan Plateau and their controlling factors, Atmos.
784 Res., 303, 10.1016/j.atmosres.2024.107328, 2024.
785 Craig, H.: Isotopic Variations in Meteoric Waters, Science, 133, 1702-1703, 10.1126/science.133.3465.1702,
786 1961.
787 Craig, H. and Gordon, L. I.: Deuterium and oxygen 18 variations in the ocean and the marine atmosphere, in:
788 Stable Isotopes in Oceanographic Studies and Paleotemperatures. Spoleto, Tongiorgi, E., Italy, 9-130, 1965.
789 Dai, D., Gao, J., Steen-Larsen, H. C., Yao, T., Ma, Y., Zhu, M., and Li, S.: Continuous monitoring of the isotopic
790 composition of surface water vapor at Lhasa, southern Tibetan Plateau, Atmos. Res., 264,
791 10.1016/j.atmosres.2021.105827, 2021.
792 Dansgaard, W.: Stable isotopes in precipitation, Tellus, 16, 436-468, 10.1111/j.2153-3490.1964.tb00181.x,
793 1964.
794 Dütsch, M., Pfahl, S., and Sodemann, H.: The impact of nonequilibrium and equilibrium fractionation on two
795 different deuterium excess definitions, J. Geophys. Res., 122, 12732-12746, 10.1002/2017JD027085, 2017.
796 Fiorella, R. P., Poulsen, C. J., and Matheny, A. M.: Seasonal Patterns of Water Cycling in a Deep, Continental
797 Mountain Valley Inferred from Stable Water Vapor Isotopes, J. Geophys. Res., 123, 7271-7291,
798 doi:10.1029/2017JD028093, 2018.
799 Galewsky, J., Steen-Larsen, H. C., Field, R. D., Worden, J., Risi, C., and Schneider, M.: Stable isotopes in
800 atmospheric water vapor and applications to the hydrologic cycle, Rev. Geophys., 54, 809-865,
801 10.1002/2015RG000512, 2016.
802 Good, S. P., Noone, D., and Bowen, G.: Hydrologic connectivity constrains partitioning of global terrestrial
803 water fluxes, Science, 349, 175-177, 10.1126/science.aaa5931, 2015.
804 Guo, H., Pang, H., Wu, S., Xu, T., Mutz, S. G., Zhan, Z., Lin, W., Zhang, W., and Hou, S.: Global abnormal
805 precipitation 18O depletion during late/post monsoon season, Earth Planet. Sci. Lett., 641,
806 10.1016/j.epsl.2024.118815, 2024.
807 Han, J., Tian, L., Cai, Z., Ren, W., Liu, W., Li, J., and Tai, J.: Season-specific evapotranspiration partitioning using
808 dual water isotopes in a Pinus yunnanensis ecosystem, southwest China, J. Hydrol., 608, 127672,

10.1016/j.jhydrol.2022.127672, 2022.

He, S., Jackisch, D., Feng, L., Samanta, D., Wang, X., and Goodkin, N. F.: Uncovering Below Cloud Rain-Vapor Interactions During Tropical Rain Events Through Simultaneous and Continuous Real-Time Monitoring of Rain and Vapor Isotopes, J. Geophys. Res., 129, e2023JD040084, https://doi.org/10.1029/2023JD040084, 2024.

He, Y., Risi, C., Gao, J., Masson-Delmotte, V., Yao, T., Lai, C.-T., Ding, Y., Worden, J., Frankenberg, C., Chepfer, H., and Cesana, G.: Impact of atmospheric convection on south Tibet summer precipitation isotopologue composition using a combination of in situ measurements, satellite data and atmospheric general circulation modeling, J. Geophys. Res., 120, 3852-3871, 10.1002/2014JD022180, 2015.

Hersbach, H., Bell, B., Berrisford, P., Horányi, A., J., M.-S., Nicolas, J., Radu, R., Schepers, D., Simmons, A., Soci, C., and Dee, D.: Global reanalysis: goodbye ERA-Interim, hello ERA5, 10.21957/vf291hehd7, 2019.

Huang, J.: A Simple Accurate Formula for Calculating Saturation Vapor Pressure of Water and Ice, Journal of Applied Meteorology and Climatology, 57, 1265-1272, https://doi.org/10.1175/JAMC-D-17-0334.1, 2018.

Huffman, G. J., Stocker, E. F., Bolvin, D. T., Nelkin, E. J., and Tan, J.: GPM IMERG Final Precipitation L3 Half Hourly 0.1 degree x 0.1 degree V07, Greenbelt, MD, Goddard Earth Sciences Data and Information Services Center (GES DISC) [dataset], 10.5067/GPM/IMERG/3B-HH/07, 2023.

Immerzeel, W. W., Lutz, A. F., Andrade, M., Bahl, A., Biemans, H., Bolch, T., Hyde, S., Brumby, S., Davies, B. J., Elmore, A. C., Emmer, A., Feng, M., Fernández, A., Haritashya, U., Kargel, J. S., Koppes, M., Kraaijenbrink, P. D. A., Kulkarni, A. V., Mayewski, P. A., Nepal, S., Pacheco, P., Painter, T. H., Pellicciotti, F., Rajaram, H., Rupper, S., Sinisalo, A., Shrestha, A. B., Viviroli, D., Wada, Y., Xiao, C., Yao, T., and Baillie, J. E. M.: Importance and vulnerability of the world's water towers, Nature, 577, 364-369, 10.1038/s41586-019-1822-y, 2020.

Jiang, J., Zhou, T., Qian, Y., Li, C., Song, F., Li, H., Chen, X., Zhang, W., and Chen, Z.: Precipitation regime changes in High Mountain Asia driven by cleaner air, Nature, 10.1038/s41586-023-06619-y, 2023.

Joswiak, D. R., Yao, T., Wu, G., Tian, L., and Xu, B.: Ice-core evidence of westerly and monsoon moisture contributions in the central Tibetan Plateau, J. Glaciol., 59, 56-66, 10.3189/2013JoG12J035, 2013.

Keeling, C. D.: The concentration and isotopic abundances of atmospheric carbon dioxide in rural areas, Geochim. Cosmochim. Acta, 13, 322-334, 10.1016/0016-7037(58)90033-4, 1958.

Kurita, N., Noone, D., Risi, C., Schmidt, G. A., Yamada, H., and Yoneyama, K.: Intraseasonal isotopic variation associated with the Madden-Julian Oscillation, J. Geophys. Res., 116, D24101, 10.1029/2010JD015209, 2011.

Lawrence, J. R., Gedzelman, S. D., Dexheimer, D., Cho, H.-K., Carrie, G. D., Gasparini, R., Anderson, C. R., Bowman, K. P., and Biggerstaff, M. I.: Stable isotopic composition of water vapor in the tropics, J. Geophys. Res., 109, D06115, 10.1029/2003JD004046, 2004.

Lee, J.-E. and Fung, I.: "Amount effect" of water isotopes and quantitative analysis of post-condensation processes, Hydrol. Processes, 22, 1-8, 10.1002/hyp.6637, 2008.

Liu, F., Tian, L., Cai, Z., Wang, X., Liang, P., Wang, S., and Li, S.: What caused the lag between oxygen-18 and deuterium excess in atmospheric vapor and precipitation during the earlier summer season in southwest China?, J. Hydrol., 644, 10.1016/j.jhydrol.2024.132087, 2024.

Liu, J., Xiao, C., Ding, M., and Ren, J.: Variations in stable hydrogen and oxygen isotopes in atmospheric water vapor in the marine boundary layer across a wide latitude range, Journal of Environmental Sciences, 26, 2266-2276, 10.1016/j.jes.2014.09.007, 2014.

Luo, L.: Meteorological observation data from the integrated observation and research station of the alpine environment in Southeast Tibet (2007-2017), National Tibetan Plateau Data Center [dataset], 10.11888/AtmosphericPhysics.tpe.68.db, 2018.

Ma, T., Jiang, Z., Ding, M., He, P., Li, Y., Zhang, W., and Geng, L.: A model framework for atmosphere–snow water vapor exchange and the associated isotope effects at Dome Argus, Antarctica – Part 1: The diurnal changes,

The Cryosphere, 18, 4547-4565, 10.5194/tc-18-4547-2024, 2024.

Merlivat, L. and Jouzel, J.: Global climatic interpretation of the deuterium-oxygen 18 relationship for precipitation, J. Geophys. Res., 84, 5029-5033, 1979.

Noone, D.: Pairing Measurements of the Water Vapor Isotope Ratio with Humidity to Deduce Atmospheric Moistening and Dehydration in the Tropical Midtroposphere, J. Climate, 25, 4476-4494, 10.1175/jcli-d-11-00582.1, 2012.

Pang, H., Hou, S., Kaspari, S., Mayewski, P., Introne, D., Masson-Delmotte, V., Jouzel, J., Li, Z., He, Y., Hong, S., and Qin, D.: Atmospheric circulation change in the central Himalayas indicated by a high-resolution ice core deuterium excess record, Climate Research, 53, 1-12, 10.3354/cr01090, 2012.

Putman, A. L., Fiorella, R. P., Bowen, G. J., and Cai, Z.: A Global Perspective on Local Meteoric Water Lines: Meta-analytic Insight into Fundamental Controls and Practical Constraints, Water Resour. Res., 55, 6896-6910, 10.1029/2019wr025181, 2019.

Risi, C., Bony, S., and Vimeux, F.: Influence of convective processes on the isotopic composition ($\delta^{18}O$ and $\delta D$) of precipitation and water vapor in the tropics: 2. Physical interpretation of the amount effect, J. Geophys. Res., 113, D19306, 10.1029/2008JD009943, 2008a.

Risi, C., Bony, S., Vimeux, F., Descroix, L., Ibrahim, B., Lebreton, E., Mamadou, I., and Sultan, B.: What controls the isotopic composition of the African monsoon precipitation? Insights from event-based precipitation collected during the 2006 AMMA field campaign, Geophys. Res. Lett., 35, L24808, 10.1029/2008GL035920, 2008b.

Ruan, J., Zhang, H., Cai, Z., Yang, X., and Yin, J.: Regional controls on daily to interannual variations of precipitation isotope ratios in Southeast China: Implications for paleomonsoon reconstruction, Earth Planet. Sci. Lett., 527, 115794, 10.1016/j.epsl.2019.115794, 2019.

Samuels-Crow, K. E., Galewsky, J., Sharp, Z. D., and Dennis, K. J.: Deuterium excess in subtropical free troposphere water vapor: Continuous measurements from the Chajnantor Plateau, northern Chile, Geophys. Res. Lett., 41, 8652-8659, 10.1002/2014gl062302, 2014.

Sayres, D. S., Pfister, L., Hanisco, T. F., Moyer, E. J., Smith, J. B., St. Clair, J. M., O'Brien, A. S., Witinski, M. F., Legg, M., and Anderson, J. G.: Influence of convection on the water isotopic composition of the tropical tropopause layer and tropical stratosphere, J. Geophys. Res., 115, 10.1029/2009JD013100, 2010.

Scholl, M. A., Shanley, J. B., Zegarra, J. P., and Coplen, T. B.: The stable isotope amount effect: New insights from NEXRAD echo tops, Luquillo Mountains, Puerto Rico, Water Resour. Res., 45, 10.1029/2008wr007515, 2009.

Shao, L., Tian, L., Cai, Z., Wang, C., and Li, Y.: Large-scale atmospheric circulation influences the ice core d-excess record from the central Tibetan Plateau, Clim. Dyn., 57, 1805-1816, 10.1007/s00382-021-05779-9, 2021.

Sodemann, H., Schwierz, C., and Wernli, H.: Interannual variability of Greenland winter precipitation sources: Lagrangian moisture diagnostic and North Atlantic Oscillation influence, J. Geophys. Res., 113, 10.1029/2007jd008503, 2008.

Sodemann, H., Aemisegger, F., Pfahl, S., Bitter, M., Corsmeier, U., Feuerle, T., Graf, P., Hankers, R., Hsiao, G., Schulz, H., Wieser, A., and Wernli, H.: The stable isotopic composition of water vapour above Corsica during the HyMeX SOP1 campaign: insight into vertical mixing processes from lower-tropospheric survey flights, Atmos. Chem. Phys., 17, 6125-6151, 10.5194/acp-17-6125-2017, 2017.

Steen-Larsen, H. C., Risi, C., Werner, M., Yoshimura, K., and Masson-Delmotte, V.: Evaluating the skills of isotope-enabled General Circulation Models against in-situ atmospheric water vapor isotope observations, J. Geophys. Res., 122, 246-263, 10.1002/2016JD025443, 2017.

Stein, A. F., Draxler, R. R., Rolph, G. D., Stunder, B. J. B., Cohen, M. D., and Ngan, F.: NOAA's HYSPLIT atmospheric transport and dispersion modeling system, Bull. Am. Meteorol. Soc., 96, 2059-2077, 10.1175/BAMS-D-14-00110.1, 2015.

Terzer-Wassmuth, S., Wassenaar, L. I., Welker, J. M., and Araguas-Araguas, L. J.: Improved High-Resolution Global and Regionalized Isoscapes of δ18O, δ2H, and d-Excess in Precipitation, Hydrol. Processes, 35, 10.1002/hyp.14254, 2021.

Thompson, L. G., Yao, T., E.Mosley-Thompson, Davis, M. E., Henderson, K. A., and Lin, P.-N.: A High-Resolution Millennial Record of the South Asian Monsoon from Himalayan Ice Cores, Science, 289, 1916-1919, 10.1126/science.289.5486.1916, 2000.

Thompson, L. G., Yao, T. D., Davis, M. E., Mosley-Thompson, E., Synal, H. A., Wu, G., Bolzan, J. F., Kutuzov, S., Beaudon, E., Sierra-Hernández, M. R., and Beer, J.: Ice core evidence for an orbital-scale climate transition on the Northwest Tibetan Plateau, Quat. Sci. Rev., 324, 10.1016/j.quascirev.2023.108443, 2024.

Tian, L., Masson-Delmotte, V., Stievenard, M., Yao, T., and Jouzel, J.: Tibetan Plateau summer monsoon northward extent revealed by measurements of water stable isotopes, J. Geophys. Res., 106, 28081-28088, 10.1029/2001JD900186, 2001.

Tian, L., Yao, T., MacClune, K., White, J. W. C., Schilla, A., Vaughn, B., Vachon, R., and Ichiyanagi, K.: Stable isotopic variations in west China: A consideration of moisture sources, J. Geophys. Res., 112, D10112, 10.1029/2006jd007718, 2007.

Tian, L., Yu, W., Schuster, P. F., Wen, R., Cai, Z., Wang, D., Shao, L., Cui, J., and Guo, X.: Control of seasonal water vapor isotope variations at Lhasa, southern Tibetan Plateau, J. Hydrol., 580, 124237, 10.1016/j.jhydrol.2019.124237, 2020.

Uemura, R., Matsui, Y., Yoshimura, K., Motoyama, H., and Yoshida, N.: Evidence of deuterium excess in water vapor as an indicator of ocean surface conditions, J. Geophys. Res., 113, 10.1029/2008jd010209, 2008.

Vuille, M., Bradley, R. S., Werner, M., Healy, R., and Keimig, F.: Modeling $\delta^{18}O$ in precipitation over the tropical Americas: 1. Interannual variability and climatic controls, J. Geophys. Res., 108, 4174, 10.1029/2001JD002038, 2003.

Wahl, S., Steen-Larsen, H. C., Hughes, A. G., Dietrich, L. J., Zuhr, A., Behrens, M., Faber, A.-K., and Hörhold, M.: Atmosphere-Snow Exchange Explains Surface Snow Isotope Variability, Geophys. Res. Lett., 49, e2022GL099529, 10.1029/2022GL099529, 2022.

Webster, C. R. and Heymsfield, A. J.: Water isotope ratios D/H, 18O/16O, 17O/16O in and out of clouds map dehydration pathways, Science, 302, 1742-1745, 10.1126/science.1089496, 2003.

Wei, Z. and Lee, X.: The utility of near-surface water vapor deuterium excess as an indicator of atmospheric moisture source, J. Hydrol., 123923, 10.1016/j.jhydrol.2019.123923, 2019.

Welp, L. R., Lee, X., Griffis, T. J., Wen, X. F., Xiao, W., Li, S., Sun, X., Hu, Z., Val Martin, M., and Huang, J.: A meta-analysis of water vapor deuterium-excess in the midlatitude atmospheric surface layer, Global Biogeochem. Cycles, 26, 10.1029/2011gb004246, 2012.

Worden, J., Noone, D., and Bowman, K.: Importance of rain evaporation and continental convection in the tropical water cycle, Nature, 445, 528-532, 10.1038/nature05508, 2007.

Yang, X. and Yao, T.: Seasonality of moisture supplies to precipitation over the Third Pole: a stable water isotopic perspective, Sci Rep, 10, 15020, 10.1038/s41598-020-71949-0, 2020.

Yang, X., Davis, M. E., Acharya, S., and Yao, T.: Asian monsoon variations revealed from stable isotopes in precipitation, Clim. Dyn., 51, 2267-2283, 10.1007/s00382-017-4011-4, 2017.

Yao, T., Masson-Delmotte, V., Gao, J., Yu, W., Yang, X., Risi, C., Sturm, C., Werner, M., Zhao, H., He, Y., Ren, W., Tian, L., Shi, C., and Hou, S.: A review of climatic controls on $\delta^{18}O$ in precipitation over the Tibetan Plateau: Observations and simulations, Rev. Geophys., 51, 525-548, 10.1002/rog.20023, 2013.

Yao, T., Bolch, T., Chen, D., Gao, J., Immerzeel, W., Piao, S., Su, F., Thompson, L., Wada, Y., Wang, L., Wang, T., Wu, G., Xu, B., Yang, W., Zhang, G., and Zhao, P.: The imbalance of the Asian water tower, Nature Reviews Earth & Environment, 3, 618-632, 10.1038/s43017-022-00299-4, 2022.

Yu, W., Tian, L., Ma, Y., Xu, B., and Qu, D.: Simultaneous monitoring of stable oxygen isotope composition in water vapour and precipitation over the central Tibetan Plateau, Atmos. Chem. Phys., 15, 10251-10262, 10.5194/acp-15-10251-2015, 2015.

Yu, W., Tian, L., Risi, C., Yao, T., Ma, Y., Zhao, H., Zhu, H., He, Y., Xu, B., Zhang, H., and Qu, D.: $\delta^{18}O$ records in water vapor and an ice core from the eastern Pamir Plateau: Implications for paleoclimate reconstructions, Earth Planet. Sci. Lett., 456, 146-156, 10.1016/j.epsl.2016.10.001, 2016.

Zhang, Q., Shen, Z., Pokhrel, Y., Farinotti, D., Singh, V. P., Xu, C.-Y., Wu, W., and Wang, G.: Oceanic climate changes threaten the sustainability of Asia's water tower, Nature, 615, 87-93, 10.1038/s41586-022-05643-8, 2023.

Zhang, Q., Shen, Z., Pokhrel, Y., Farinotti, D., Singh, V. P., Xu, C.-Y., Wu, W., and Wang, G.: Reply to: Atlantic oceanic droughts do not threaten Asian water tower, Nature, 638, E16-E18, 10.1038/s41586-024-08358-0, 2025.

Zhao, H., Xu, B., Li, Z., Wang, M., Li, J., and Zhang, X.: Abundant climatic information in water stable isotope record from a maritime glacier on southeastern Tibetan Plateau, Clim. Dyn., 48, 1161-1171, 10.1007/s00382-016-3133-4, 2017.

Zhao, H., Xu, B., Yao, T., Wu, G., Lin, S., Gao, J., and Wang, M.: Deuterium excess record in a southern Tibetan ice core and its potential climatic implications, Clim. Dyn., 38, 1791-1803, 10.1007/s00382-011-1161-7, 2012.

Zhao, Y., Xu, C., Yu, X., Liu, Y., and Ji, X.: Atlantic oceanic droughts do not threaten Asian water tower, Nature, 638, E13-E15, 10.1038/s41586-024-08357-1, 2025.